INSTITUTO POLITÉCNICO DE BRAGANÇA
Escola Superior de Tecnologia e Gestão

Development and functionalization of magnetic nanocomposites for cancer treatment

Jessica do Rocio de Paula de Oliveira

Thesis presented to the

Escola Superior de Tecnologia e Gestão

Polytechnic Institute of Bragança

To obtain the Master degree in

Chemical Engineering

Supervisor:

Dr. Helder Gomes (IPB)

Co-supervisor:

Dr. Luís Fernando Marchesi (UTFPR)

September/2017

INSTITUTO POLITÉCNICO DE BRAGANÇA
Escola Superior de Tecnologia e Gestão

Development and functionalization of magnetic nanocomposites for cancer treatment

Jessica do Rocio de Paula de Oliveira

Thesis presented to the

Escola Superior de Tecnologia e Gestão

Polytechnic Institute of Bragança

To obtain the Master degree in

Chemical Engineering

September/2017

To my family

Acknowledgement

Many people have facilitated the preparation of this work for both practical and scientific support as well as in an emotional and affective way. In this way, I extend my acknowledgement to all who have been with me throughout this research.

I thank the professors Dr. Helder T. Gomes and Dr. Luis Fernando Marchesi for the scientific support and guidance in the project, as well as the encouragement of the academic career. I am grateful to professor Dra. Isabel C. F. Ferreira for the offer of the extracts of plants so that all the work was realized; and also to the Project POCI-01-0145-FEDER-006984 – Associate Laboratory LSRE-LCM funded by FEDER through COMPETE2020 - POCI – and by national funds through FCT - Fundação para a Ciência e a Tecnologia. I also thank Isabel P. M. Fernandes for running the FT-IR tests and professor Pedro B. Tavares for the XRD and TEM analysis.

Immeasurably thanks to Raquel O. Rodrigues and Rui S. Ribeiro for all their support with the experiments and ideas for me to develop the work, for the great patience they had with me and for the bonds of friendship that we built in this time of coexistence. To Catarina and António who welcomed me and made me feel at home in Portugal: thank you. And to all the labor friends and new friendships I have made, as well as to the friends that were far away and strengthening my choice of being here: you sure make life worth living. Among the many friends who had encouraged me from distance, I need to mention Micheli Vaz Madalozo Santos, Bruno Madalozo, Matheus Mathuchenko and Bruna Soares, who, in addition to hearing me talk tirelessly about magnetic nanoparticles, were always open to my confidences and, with their words, helped me to recharge the energy I needed to continue.

Many thanks to my parents, Beatriz and Isalem, who believed and bet on my dream and made it real. I hope you are proud of my choices and that I have always honored everything I learned from you, always trying to be fair, courageous and kind. Without all the affection and encouragement I have had since birth, I would not be here today. Special thanks to my sister Renata, who even far away, had the same complicity of always, and even with the pain of longing for me, was able to give me strength when I needed.

Many thanks, with love, to my boyfriend, Igor N. Buss, for being so special at this important moment of my life, for not ceasing to love me, for not giving up our relationship even with many obstacles, and for reading my thesis so many times, helping me with tips and corrections. You are to me the great proof that with love and patience we can win many things.

I thank God above all, who was present at every moment and in the most sincere prayers looked at me. He provided everything at the right moment, giving me this project that I loved to work on, putting all these wonderful people in my path and helping me to be able to accomplish the goals, to get here and certainly to continue with all that He will give me at the right moment.

Abstract

Green routes, considering the use of plant extracts with high reducing power, have been investigated as alternative methods to obtain superparamagnetic cores for biomedical applications. Usually, these magnetic cores are further coated either with metal or non-metal materials. In particular, carbon-coated nanoparticles have several advantages in comparison to other coatings, since they usually offer higher chemical and thermal stability, larger surface area, biocompatibility and easier functionalization. In this research, different plant hydromethanolic extracts with high reducing power (i.e., *Tamus communis* L. shoots, *Crateagus monogyna* Jacq. flowers and *Rubus ulmifolius* Schott flowers) were investigated in the synthesis of magnetic cores for carbon-coated yolk-shell magnetic nanoparticles (CYSMNPs). Overall, the extract of *Rubus ulmifolius* has shown great ability to produce highly magnetic cores with more stability in distilled water. The nanocomposites were chemically functionalized with nitric acid to enhance the colloidal stability of the product synthesized. To set the best conditions for drug loading, different working solutions (i.e., phosphate buffer solutions (PBS) pH 6.0, pH 7.4 and pH 8.0) were investigated. It is known that there are differences between the pH of the normal tissues (pH 7.4), the extracellular environment of the tumor (pH 6.5) and the endosome and lysosome (pH lower than 5.0). Then, according to the best loading, the drug release was also studied in different working solutions (i.e., PBS pH 4.5, PBS pH 6.0 and PBS pH 7.4), to determine the efficiency of the synthesized material for drug delivery in cells targeted to cancer treatment. The results showed a drug release quantity 20% higher in acid environment than in neutral environment. However, this research demonstrates the outstanding ability to use the developed and optimized green CYSMNPs, as super-drug nanocarriers with great ability to load high content of the anticancer drug Doxorubicin.

Resumo

As rotas verdes, considerando o uso de extratos de plantas com elevado poder redutor, foram investigadas como métodos alternativos para a obtenção de núcleos superparamagnéticos para aplicações biomédicas. Geralmente, esses núcleos magnéticos são revestidos com materiais metálicos ou não metálicos. Em particular, nanopartículas revestidas com materiais de carbono têm várias vantagens em comparação com outros revestimentos, uma vez que geralmente oferecem maior estabilidade química e térmica, maior área superficial, biocompatibilidade e facilidade de funcionalização. Neste trabalho, foram investigados diferentes extratos hidrometanólicos de plantas com alto poder redutor (i.e., brotos de *Tamus communis* L., flores de *Crateagus monogyna* Jacq e flores de *Rubus ulmifolius* Schott) na síntese de núcleos magnéticos para nanopartículas magnéticas do tipo "yolk-shell" revestidas com carbono (CYSMNPs). Em geral, o extrato de *Rubus ulmifolius* mostrou grande capacidade para produzir núcleos fortemente magnéticos e com maior estabilidade em água destilada. Os nanocompósitos foram funcionalizados quimicamente com ácido nítrico para aumentar a estabilidade coloidal do produto sintetizado. Para estabelecer as melhores condições para o carregamento do fármaco foram investigadas diferentes soluções de trabalho (i.e., PBS pH 6,0, PBS pH 7,4, PBS pH 8,0). Sabe-se que há diferenças entre o pH dos tecidos normais (pH 7,4), o ambiente extracelular do tumor (pH 6,5) e o endossoma e lisossoma (pH menor que 5,0). Em seguida, a partir do melhor carregamento, foi estudada a liberação do fármaco também em diferentes soluções de trabalho (i.e., PBS pH 4,5, PBS pH 6,0, PBS pH 7,4), para determinar a eficiência do material sintetizado para administração de fármaco em células alvo para o tratamento de câncer. Os resultados mostraram que houve uma quantidade de liberação de fármaco 20% maior em ambiente ácido do que em ambiente neutro. No entanto, esta pesquisa demonstra a excelente capacidade de usar as CYSMNP ecológicas desenvolvidas e otimizadas, como nanotransportadores de com grande capacidade de carregar um elevado conteúdo do fármaco anticancerígeno Doxorrubicina.

Index of tables

Index of figures

Summary

Chapter 1: Introduction

1.1 Introduction

Nanomaterials have been studied in the last decades for different applications. The search to synthesize materials with controlled shape and size, which can present specificity for some biomedical applications has united several areas, such as biomedicine, chemical, physics, engineering, biology and pharmaceutical [1]. Among the applications are medical diagnosis and therapy, target drug delivery [2], magnetic resonance imaging (MRI) [3] and cancer hyperthermia treatment [1,4]. Several methods to synthesize these nanomaterials have been developed with the desire to find some alternatives that are applicable, efficient and with minimal side effects. The methods of synthesis currently known are microemulsion, thermal decomposition, solvothermal, sonochemical, microwave-assisted, chemical vapor deposition, combustion synthesis, carbon arc, laser pyrolysis synthesis, co-precipitation and green routes [5,6].

Green routes are alternative and environmentally friendly ways to synthesize magnetic nanoparticles (MNPs) [7,8]. In this method, plant extracts are used to prepare the magnetic core and there are no harmful agents to be discarded. The plant extracts with high reducing power are able to promote the iron ions reduction and form oxides in a basic solution [6]. The magnetic cores synthesized are coated with carbon in yolk-shell structures. The carbon-based coating, in relation to other coatings, shows better chemical and physical properties. Generally, these nanocomposites have high surface area, are chemically inert, are biocompatible, have thermal stability and electrical conductivity [9], which are desirable for biomedical applications.

In addition to coating, the carbon-based yolk-shell magnetic nanoparticles (CYSMNPs) were functionalized with nitric acid to enhance the colloidal stability by the incorporation of carboxylic acid groups on the carbon-based shell. The functionalization leads to a dramatic change on the sample pH_{PZC} values from highly basic to highly acid, before and after the treatment, respectively. The resultant CYSMNPs are negatively charged, enabling them to have great affinity with cationic drugs, such as Doxorubicin. The electronic affinity between both can be different in solutions with different pH. Such difference can facilitate both the drug loading and the drug release depending on the solution that will be used.

However, due to this behavior, it is possible to study the optimization of the magnetic core production, coating and functionalization efficiency and the drug loading

and release environment, focusing on the release of higher amount of drug into acid environment (pH 4.5) simulating cancer cells and on the minimization of side effects in other cells, represented by slightly basic environment (pH 7.4).

1.2 Objective

The main objective of this thesis is the development and functionalization of intelligent magnetic nanostructures coated with carbon materials with high potential for the treatment of cancer through the controlled release of drugs. The magnetic core will be developed by a green route, where the biosynthesis of MNPs will be obtained by reduction of Fe (II) and Fe (III) using extracts of plants with high reducing power and ammonium hydroxide solution. This green methodology has already proven to have advantages over other chemical synthesis methodologies, namely in the obtention of more biocompatible NPs coated with biomolecules, such as polyphenols, which gives a more hydrophilic behavior and increases their colloidal stability, essential characteristics in biomedical applications [6,9]. After the NPs synthesis and functionalization to provide the magnetic nanocomposites, the purpose will be to carry out controlled drug release tests, using Doxorubicin under different conditions, mainly altering the pH of the medium. Thus, controlling the pH of the medium, the drug would not exert side effects on normal cells [10,11].

Chapter 2: State of the art

2.1 Magnetic nanoparticles

At the beginning of the 21st century, there was an increase in the production and study of the nanometer-scale materials. The development and handling of these materials are studied in nanotechnology, the science that deals with structures between 1 and 100 nanometers (nm). The nanoparticles (NPs) are structures that have nanometer scales equal to or less than 100 nm (1 nm = 10^{-9} m) [12,13]. The Magnetic Nanoparticles (MNPs) started to be researched around the 1930s, when the concept of particles with magnetic domain was discussed by William Fuller Brown and Louis Néel. The meaning of the magnetic domain particles is that all the "spins" of the particle have the same direction when subjected to a magnetic field [14].

The behavior of magnetic materials is classified based on their response to an external magnetic field. The description of magnetic field directions in the material helps to identify the different forms of magnetism. The three basic types of magnetism are diamagnetism, paramagnetism and ferromagnetism. The latter has two categories which are antiferromagnetism and ferrimagnetism [15–17].

For pharmaceutical and medical applications, mainly in cancer therapy, the combination of magnetic nanoparticles with magnetic field is promising. Because with magnetic field it is possible to focus on the target cells, minimizing the side effects of the usual treatments, such as chemotherapy [18]. The magnetic properties of these nanoparticles can be applied in magnetic resonance imaging (MRI) agents, hyperthermia agents (applying a high frequency magnetic field to selectively heat the NPs), or targeted drug delivery (a magnetic field gradient can direct magnetic vectors toward a given location for the drug release) [1–4,19]. The main materials used for this purpose include metals or metal oxides, such as iron oxide nanoparticles [18].

The main iron oxide nanoparticles are hematite (α-Fe_2O_3), magnetite (Fe_3O_4) and maghemite (γ-Fe_2O_4). NPs of those materials have been most investigated due to the diversity of possible applications. The superparamagnetic iron oxide nanoparticles (SPION) can be easily synthesized and generally are coated in the end of the process. The coating can make it viable to the desirable application reducing the potential of aggregation and avoiding the direct contact with the body. Moreover, the coating is very important to decrease the toxicity and improve the biocompatibility of these materials [3,17].

2.1.5 Nanocomposites

Nanocomposites (NCs) are multi-phasic materials, whose matrix material incorporates units with dimension less than 100 nm. The properties of these material are a combination of the properties of both the matrix material and the nanosized filler. The interaction between a magnetic field gradient and the magnetic moments of the particles induces magnetomechanical forces, which can modify the format of the host materials or displace the material [20].

According to Wen-jing Liu *et al.* (2014), the coatings of polymers, silica, carbon, or other materials over the magnetic particles can prevent aggregation, improve stabilization against degradation and functionalize the MNPs to extend their applications. The applications of nanocomposites are diverse, such as in magnetic separation, as catalyst supports, adsorbents, nanoheaters, lithium-ion batteries, supercapacitors and drug delivery agents [9,20].

2.2 Methods of synthesis

Several methods of MNPs synthesis have been studied in recent years, due to their potential applications. The choice of method depends on the different phases and the final desired compound. The most common nanoparticles are pure metals, such as Fe, Co and Ni; metallic oxides, like Fe_3O_4 and γ-Fe_2O_3; ferrites, like XFe_2O_4 (X can be Cu, Ni, Mn, Mg, among other metals); or alloys, such as FePt and CoPt. The main methods to synthesize MNPs are microemulsion, thermal decomposition, solvothermal, sonochemical, microwave-assisted, chemical vapor deposition, combustion synthesis, carbon arc, laser pyrolysis synthesis, co-precipitation and green routes [5].

2.2.1 Microemulsion

The water-in-oil (w/o) microemulsion is used to synthesize uniform sized MNPs, between 5 and 50 nm [5,21]. In this method the MNPs are synthesized in reverse micelles, which are small reactors [21]. Micelles are responsible for solubilization of organic compounds in water (oil-in-water, o/w) or hydrophilic compounds in the oil phase (w/o).

The surfactant has a hydrophobic tail and, due to that, it is a good emulsifier molecule [22]. This system is isotropic and thermodynamically stable and consists in a two-phase system that contains three compounds: water, oil and surfactant (amphiphilic molecule). The surfactant molecule allows the formation of a transparent solution resulting from the reduction of interfacial tension between water and oil. Therefore, numerous drops of water will be distributed in the organic compound (oil) [5].

The shape and size of the nanoparticles depend of the dimensions and shape of the water drop, which can be controlled by microemulsion method parameters. These parameters can be the type of surfactant and organic compound, the ratio surfactant/water/organic compound, the efficiency of surfactant for the size and shape of water drop desired, type and concentration of the reagents (salts and reducing agents), temperature, pH, method of mixture, mode and time of stirring [21].

2.2.2 Thermal decomposition

The high-temperature decomposition of organometallic precursors can result in the production of nanoparticles with size control and high level of monodispersity, between 5 and 11 nm. The homogeneous size is expected to contribute to a better controlled distribution of physical parameters [23]. These organometallic compounds can be $[X^{n+}(acac)_n]$, where X is the metal (e.g., Fe, Mn, Co, Ni and Cr), with *n* equal to 2 or 3, and *acac* is acetylacetonate; $X^y(cup)_y$, in which *cup* is N-nitrosophenylhydroxylamine; or carbonyls such as $Fe(CO)_5$. This synthesis uses organic solvents and surfactants like fatty acids, oleic acid and hexadecylamine [5].

If the organometallic precursors have zerovalent metal in their composition, then they will initially produce metallic NPs, which could be oxidized, leading to high quality monodispersed metal oxides. Otherwise, decomposition of precursors with cationic metal centers (M^{n+}) leads directly to metal oxides NPs. The size and shape of MNPs will depend on reagents (starting reagents, organometallic compounds, surfactants and solvents), temperature and time of reaction [5,23].

2.2.3 Hydrothermal and solvothermal routes

The hydrothermal route is another alternative to synthesize MNPs. This reaction occurs in reactors or autoclaves in aqueous medium with high pressure and temperature [5]. The method can be called solvothermal, to include all other solvents that can be used in the process [24]. This method of MNPs Fe_3O_4 production uses an iron source (commonly, $FeCl_3.6H_2O$), a surfactant as a protective agent (polyethylene glycol – PEG; sodium dodecyl sulfate – SDS; ethylene glycol – EG) and an alkali source and electrostatic stabilizer (sodium acetate) [5,25,26].

The solvothermal technique has high efficiency, however an important disadvantage is the slow reaction kinetics at any temperature. Microwave heating is sometimes used to increase the kinetics of crystallization [5]. The diameter of the NPs of magnetite produced by the solvothermal method can be adjustable between 120-400 nm [25]. Furthermore, mixing of SDS and PEG results in smaller (15-190 nm) and more uniform NPs, but their size depends on reaction time, initial concentration of reagents, molar ratio of reagents, protective reagents, among other factors [26].

2.2.4 Sonochemical

The sonochemical process occurs due to the phenomena of acoustic cavitation. It is attractive because of its short time of reaction, and needs demanding conditions such as high local temperature (> 5000 K), pressure (> 20 MPa), and high cooling rates (> 1010 $K.s^{-1}$) [5,27]. The acoustic cavitation consists in the formation, growth and implosive collapse of bubbles in liquids irradiated with high-intensity ultrasound [28]. The implosive collapsing of the bubbles generate a short-lived localized hotspot through adiabatic compression or shock wave formation within the gas phase of the collapsing bubble [5,28]. Kim et. al. (2005) [29] used reagents like $FeCl_3.6H_2O$, $FeCl_2.4H_2O$, $C_{18}H_{34}O_2$, NH_4OH and NaOH and they synthesized superparamagnetic iron oxide NPs with dimensions of approximately 15 nm.

2.2.5 Microwave

The microwave route is a fast, homogeneous and reproducible process to obtain iron oxide NPs, in which the concentration of the precursor, the time of irradiation and

the power are critical factors to the control of size. The sizes of the NPs obtained using this method generally are less than 10 nm [30]. The advantages of this synthesis are the fast volumetric heating, high reaction rate, reduction of reaction time and the increase of the product yield (when compared with other conventional methods of heating), besides being more environmentally friendly [31].

2.2.6 Chemical vapour deposition

Chemical vapour deposition (CVD) can be defined as the deposition of a solid in a heated surface by chemical reaction in vapour phase. Processes such as thermal decomposition (pyrolysis), reduction, hydrolysis, disproportionation, oxidation, among other reactions, are necessary for the precipitation of solid products to occur in vapour phase [5,31]. In this process, a carrier gas stream with precursors are feed continuously by a gas delivery system to a reaction chamber maintained under vacuum at high temperature (> 900 ºC). The reaction occurs in this chamber and the products combine to form clusters of NPs. The rapid expansion at the outlet of the reaction chamber causes growth and agglomeration of the particles [5].

The CVD by the reaction of a halide employed to deposit iron oxide, commonly uses iron chloride III with water at 800-1000 ºC. The efficiency of this method depends on the low concentration of the precursor in the carrier gas, and on the rapid expansion and quenching of the nucleated clusters or nanoparticles as they exit from the reactor [5]. One disadvantage is the better versatility at temperatures above 600 °C, since many substrates are not thermally stable at these temperatures. Furthermore, there is the requirement of having chemical precursors with high vapor pressure which are often hazardous and at times extremely toxic, and the by-products of the reactions are also toxic and corrosive and must be neutralized, which can be costly [31].

2.2.7 Solution combustion synthesis

The solution combustion synthesis (SCS) is an exothermal redox reaction between an oxidizer (like metal nitrates) and a fuel (e.g., glycine, urea and citric acid). The advantages of the SCS are the resulting NPs with high specific surface area and high

reactivity, the use of inexpensive starting reagents, the self-sustained instantaneous reactions and the resultant high yield [32].

2.2.8 Plasma arc discharge

The plasma arc discharge (PAD) is used to synthesize ultra-fine powders of magnetic oxides. In this method, the nanoparticles are immediately produced after the establishment of the arc between two electrodes. Some advantages are the ultra-fine MNP size with high purity and the high industrial scale production capacity. To control the desired size of the nanoparticles, some parameters are set such as arc discharge current, air chamber atmosphere and chamber pressure [33]. The PAD method is used to synthesize MNPs coatings by carbon [5].

2.2.9 Laser pyrolysis

The synthesis of MNPs by the method of laser pyrolysis is promising, due to the efficiency of the process in the production of small sized particles and narrow size distribution (between 2-7 nm) [5,34,35]. The laser pyrolysis is based on the resonant interaction between laser photons and at least one gaseous species – reactants or sensitizer [34]. This type of synthesis is used to prepare iron-based nanostructures [5].

2.2.10 Co-precipitation

With the co-precipitation method it is possible to synthesize oxides and ferrites by addition of a strong base on iron salts [5]. The reaction can be represented by equation (1) where X can be Fe, Mn, Co, Cu, Mg, Zn and Ni. At the end of the precipitation it is expected that the solution pH stays between 8 and 14, with a stoichiometric ratio of 2:1 (Fe^{2+}/X^{2+}) [5].

$$X^{2+} + 2Fe^{3+} + 8OH^{-} \rightarrow XFe_2O_4 + 4H_2O \qquad (1)$$

Magnetite nanoparticles (Fe_3O_4) are stable in environmental conditions, so they can be oxidized to maghemite (γ-Fe_2O_3) or dissolved in acidic medium. The size, shape

and composition of the MNPs will depend on some factors such as the type of salts used (e.g., chlorides, sulfates and nitrates), the reaction temperature, the pH value, the type and strength of the base, the mixing rate, the ionic strength of the medium and the Fe^{2+}/X^{2+} ratio [5]. Hong *et al* (2008) used NH_4OH instead of NaOH and they concluded that the NH_4OH solution provides to NPs better crystallinity, smaller size and higher saturation magnetization [36].

2.2.11 Reducing using plants extract

Green synthesis or biosynthesis is a method that uses plant extract to produce MNPs. Several types of extracts have already been applied in this method, such as leaves, seeds and fruit extracts. Among the species already analyzed the following can be cited: *Amaranthus dubius* [37], *Euphorbia milli, Datura innoxia, Calotropis procera, Tinospora cordifolia, Tridax procumbens and Cymbopogon citratus* [7]; *Salvia officinalis* [38]; *Hordeum vulgare* and *Rumex acetosa* [39]; *Castanea sativa, Eucalyptus globulus, Ulex europaeus* and *Pinus pinaster* [40]; *Citrullus lanatus* [41] and green tea extract [42,43].

In this type of synthesis the size and shape of NPs will depend on the characteristics of the extract, its localization in the plant, the reaction temperature, the stirring, the pH, and the biologic composition of plant (such as flavonoids, terpenoids, amino acids proteins, sugars) [44]. In general , the size can vary between 2 and 40 nm [6,7,37–42,45].

Typically, the green synthesis is made only by adding the plant extract in a solution containing Fe (III) and/or Fe (II) at room temperature and stirring for a given time [37–40,45,46]. However, to obtain NPs with the desired size the reaction temperature must be well controlled [7,41,42,44].

Because it does not use many reagents and do not discard harmful components during the washing, this synthesis received the name of green synthesis or green route. Otherwise, there is the possibility of using a concentrated basic solution added to mixture of the iron solution with vegetal extract [6,8,47]. So, it will be similar to the synthesis by co-precipitation, but the NPs are coated by vegetal extract [6].

In this thesis, it was chosen to use the methods of synthesis green routes and co-precipitation to produce magnetite. Because of the possibility of using new plant extracts

for synthesis and environment friendly characteristic of the first one combined with the efficiency and practicality of the last one.

2.3 Structure of nanoparticles

The structure of nanoparticles can be very different from each other, due to the type of synthesis used, the composition and their purpose. According to the structure, nanoparticles can be classified as solid nanoparticles with uniform structure, hollow particles, Janus particles, core-shell (CS) particles, reverse bumpy balls particles and yolk-shell (YS) particles. Nanoparticles are generally found in the form of spheres, but they can be also cubic, spindle or rodlike [48]. In Figure 1 is represented the structure classification of nanoparticles.

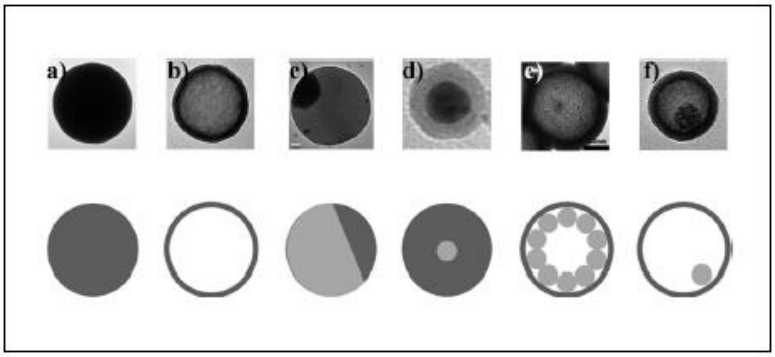

Figure 1 - Transmission Electron Microscopy (TEM) images and schematic representations of the common types of nanoparticles: a) Solid nanoparticle, b) Hollow particle, c) Janus particle, d) Core-shell particle, e) Reverse bumpy balls and f) Yolk-shell particle [48].

Usually, coated NPs are used because the coating decreases agglomeration and, in the case of biomedical applications, can improve the biocompatibility and decrease toxicity of the NPs. The coating can be polymeric or based on activated carbon, silica, gold, among other materials[17]. The coated structures more applied are core-shell and yolk-shell.

2.3.1 Core-shell

Core-shell nanoparticles (CSNPs) are a class of particles that contains a core and a shell. The core and shell can be of different materials or both of the same material with

different structures. The core may be an aggregation of several small spheres or a single sphere. The shell structure can be a continuous layer or an attachment of smaller spheres onto a big core sphere, or aggregated core spheres. Complex core-shell structures may also be produced via incorporation of smaller spheres into the shell or with multiple shells. Both the core and the shell can be nonporous solids or having desirable porous structures. The size of the core particle, the thickness of the shell and the porosity are adjusted to be suitable to different types of applications [49].

Normally, the CSNPs are synthesized by a process with two or more steps. The core particles are synthesized before and the coating is formed on the core particle using different methods, according with the type of core and coating materials, furthermore considering the morphology of the particles. The motivation in the preparation of core-shell particles is to combine the desired properties of different materials and structures in order to offer simultaneous effect, to stabilize the active particles or to provide biocompatible properties [49].

2.3.2 Yolk-shell

In the last years, the yolk-shell nanoparticles (YSNPs) already received some different terminologies, including nanorattle, movable core/shell and core/shell with hollow interiors. The main difference between the CSNPs and YSNPs is the presence of void space derived from the sacrificial layer which gives rise to the multifunctional and other unique properties of YSNPs. Therefore, YSNPs are hybrid structures consisting of a movable core inside the hollow shell of the same or different materials [50].

One of the advantages of the YS structure over the CS structure is that the first has the core surface unlocked compared to the second and, due to this, it provides more active locations and larger surface area. Moreover, the void space is suitable to accommodate the guest molecules and to provide space for the expansion of core NPs in many applications; the shell layer provides more active inner and outer surfaces, and the YSNPs can be synthesized even from a single material to enhance the specific surface area [50].

These particles can be classified as spherical or non-spherical. The spherical particles are subdivided into single core-shell, multi-cores/single shell, single core/multi-shells, multi-cores/shells and multi-shells or shell in shell. The non-spherical particles are

subdivided into partially non-spherical (where either the core or the shell of the YS has a non-spherical shape), and complete non-spherical (where both the core and the shell have a non-spherical shape) [50].

The YSNPs synthesis often involves several steps including the fabrication of the core, growth of the shell, as well as various post-synthesis treatments such as core removal, functionalization of compartments and loading with cargo [48]. In general, the synthesis of the YSNPs begins with the formation of the core (or yolk) of the structure, followed by coating with the desired material according to the application of the synthesized NPs [48,50].

Graphene or reduced graphene oxide (rGO) has been used as shell of YS structures, integrating NPs of MnO_2, Fe_3O_3, TiO_2, Pt and Ag. The reduced graphene oxide favors a better dispersion of nanoparticles, improving their catalytic activity and durability [51].

2.4 Applications

Most applications of MNPs require features such as nanomaterials with specific sizes, shapes, surface characteristics and magnetic properties, chemical stability and good dispersion in liquid media. To achieve all this, it is necessary that the nanoparticles have functionalized surfaces [1]. Thus, the surface of the MNPs must be modified with functional groups or suitable molecules, usually becoming a nanocomposite. Areas for applications of MNPs and magnetic nanocomposites are diverse, such as industrial, biochemical and biomedical [5].

2.4.1 Industrial applications

Among the many applications, MNPs can be applied to high density magnetic data storage devices, magnetic information storage, xerography, electronics, catalysis, magnetic inks, magnetic refrigeration and their systems [5]. According to Teja & Koh (2009), the particles in data storage applications must have a stable, switchable magnetic state that could not be affected by temperature fluctuations. For optimum performance in recording, the particles should exhibit both high coercivity and high remanence, and they

should be uniformly small, and resistant to corrosion, friction and temperature changes. Due to its chemical and physical stability, maghemite is useful in recording and data storage, which may be cobalt-coated, in order to improve the coercivity and storage capacity.

2.4.2 Biochemical applications

2.4.2.1 Application in catalysis

Catalysts based in MNPs have been widely used to improve the heterogeneous catalysis limitations. Such small and magnetically separable catalysts could combine the advantages of high dispersion and reactivity with easy separation. In this way, magnetically driven separations make the recovery of catalysts in a liquid-phase reaction much easier than using cross flow filtration and centrifugation, especially when the catalysts are in the nanometer size range [5].

2.4.2.2 Environmental applications

MNPs can be used as alternatives applied to the pumping and treatment of groundwater using permeable reactive barriers. Nanoparticles capable of reducing and stabilizing different types of compounds may be useful in this process, such as zero-valent iron NPs. An important property of iron nanoparticles is their enormous flexibility for *in situ* applications, but a major drawback is their sensitivity to oxidation in air and aqueous solutions. Environmental applications for MNPs include the ability of these materials to remove organic and inorganic pollutants [5].

2.4.3 Biomedical applications

2.4.3.1 Bioseparation

In the biomedical area, separation of specific biological entities (e.g., DNAs, proteins and cells) from their native environment is often required for analysis. The on-off nature of magnetization with and without an external magnetic field makes superparamagnetic colloids suitable for this situation, since they enable the transportation of biomaterials with a magnetic field. The separation processes of specific molecules are

used in almost all areas of bioscience and biotechnology. Various magnetic particles have been developed as magnetic carriers in separation processes, including purification and immunoassays. Separation techniques are extremely important in process engineering [52].

2.4.3.2 Magnetic resonance imaging

The use of nanoparticles of magnetite and maghemite has received considerable attention in the application as contrast agents by magnetic resonance imaging (MRI). This application require particles that exhibit superparamagnetic behavior at room temperature and that are stable in water at neutral pH and physiological conditions [1].

According Ito *et.al.* (2005), paramagnetic ion chelates and ferromagnetic or superparamagnetic nanoparticles, with sizes ranging generally between 3 and 10 nm, were developed as MRI contrast agents and used in clinical diagnosis. Magnetic resonance imaging offers the advantage of a high spatial resolution of contrast differences between tissues. Due to the unique function of this imaging modality, it is necessary to develop effective contrast agents that enhance and amplify their diagnostic utility [52].

2.4.3.3 Hyperthermia

Magnetic hyperthermia (MH) is a clinical therapy used along with chemotherapy to achieve a synergistic effect to the combined treatment of cancer cells. The MH process is based on increasing the temperature of the target cells to 41-46 °C. At this temperature, the damage to normal tissue is reversible, while the tumor cells are irreversibly damaged. Recently, magnetic nanoparticles (mainly magnetite) have been used as heating agents for this treatment [1,4].

In application to hyperthermia, magnetic nanoparticles, whose position and orientation can be controlled by a magnetic field, need an important requirement, which is the absorption of large losses under the reversal of repeated magnetization. The mobility of magnetic particles in ferrofluids is an important feature in the context of losses under repeated magnetization reversal. As the particles are free to rotate, the potential energy can be minimized in two ways: either the magnetic moment rotates within the particle until it is aligned with the field, or the particle rotates as a whole. Two different processes are involved to explain this, Néel and Brown relaxation, respectively. These relaxation movements cause the characteristic heating of MH [53]. The efficiency of the

transformation of magnetic field energy by physical mechanisms strongly depends on the nature of the particles, such as particle size, state of agglomeration and viscosity of the medium [1,4].

2.4.3.4 Drug delivery

The controlled transportation and release of drugs aims to avoid wasting drugs and distributing them in unnecessary areas, also avoiding unwanted side effects. The NPs containing the drug are inserted into the bloodstream and guided with the aid of a magnetic field to the "target" where the drug is released. The release may occur due to enzymatic activity, or controlled by other specific factors, for example pH. The success of this method depends on the speed of the NPs in the bloodstream, the circulation time and the strength of the magnetic field in the region of interest [17].

2.5 Drug delivery

Controlled drug delivery systems are an alternative with the potential to overcome the challenges of administering anticancer drugs. The use of nanotechnology for this purpose has been promising, given the side effects of treatments such as chemotherapy and radiotherapy and the risks of surgeries for patients. The current drawback of cancer chemotherapy is that the drugs also affect healthy tissues, have low solubility in water and are poorly bioavailable. The NPs with diameters ranging from 10 to 200 nm present promising pharmacokinetic features. Drug encapsulated NPs accumulate both passive and active mechanisms for extended and complete circulation periods, continuous drug discharge kinetics and recovery of tissues from tumor [54]. In this context, the researches concerning nanocomposites stands out as to their ability to encapsulate therapeutic mediators and to coordinate their distribution to cancer cells [9].

According to Singh & Lillard Jr.(2009), there is a great difficulty to efficiently control the release, which depends on the solubility of the drug, desorption of the surface-bound or adsorbed drug, drug diffusion through the nanoparticle matrix, nanoparticle matrix erosion or degradation and the combination of erosion and diffusion processes [55]. One of the alternatives to deliver the drug is through the changes on the pH of the medium,

since there is a difference between the pH of the normal tissues (pH 7.4), the extracellular environment of the tumor (pH 6.5) and the endosome and lysosome (pH 5.0) [56].

NPs coated with polymers, metals or non-metals fail to release the drug controllably, while graphene oxide (GO) coated NPs have this advantage. The characteristics that allow this control and ensure GO excellent biocompatibility, physiological solubility and stability are related to the carbon domain with sp^2 hybridization, to the high specific surface area and to the enriched oxygen containing groups. In addition, -COOH (carboxylic) and GO-GO bonds facilitate conjugation with various systems, imparting GO with multi-functionalities and multi-modalities [57].

The drug composed of doxorubicin hydrochloride (DOX) is an anthracycline antiblastic antibiotic isolated from cultures of *Streptomyces peucetius var. caesius*. The chemical structure of DOX is shown in Figure 2. It is soluble in water for injections and in physiological saline solution. This drug has been used successfully to produce regression in various neoplasms, such as breast cancer, lung, bladder, thyroid and ovary carcinoma, soft tissue sarcoma and bone sarcoma, Hodgkin's and non-Hodgkin's lymphomas, neuroblastoma, Wilms' tumor, acute lymphoblastic leukemia and acute myeloblastic leukemia [58].

The use of DOX is clinically limited due to the phenomena of cell resistance, strong side effects and a dose dependent cardiotoxicity. Drug targeting by binding DOX to SPION could overcome these limitations. DOX is bound to the nanoparticle surface through a pre-formed DOX–Fe^{2+} complex. The DOX-loaded SPION presents interesting properties in terms of drug loading and biological activity [10,11].

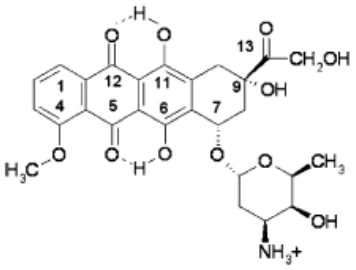

Figure 2 – Chemical structure of Doxorubicin [10].

Researches seek to improve this technique, concentrating on an efficient and specific version, minimizing the side effects that can be caused. The importance of

development and improvement for treatments of cancer is related to the cure or considerable length of life of patients. This premise is based on the world scenario, according to the World Health Organization (WHO), which reported that in 2012 there were about 14 million new cases of cancer, with forecast of 70% increase in new cases for the next two decades. In addition, this disease accounted for about 8.8 million deaths in 2015 [59]. Therefore, this report reveals the importance of improving the efficiency of treatments for cancer.

Chapter 3: Methodology

3.1 Materials

For magnetic core synthesis were used solution with iron (III) chloride 6-hydrate pure (Applichem-Panreac, Germany) and iron (II) chloride tetrahydrate (Sigma-Aldrich, Germany) as iron source for magnetite formation. Ammonium hydroxide solution 1 molar (from ammonia solution 25%, Applichem-Panreac, Germany) was used to enable co-precipitation of nanoparticles. In the early stages of the coating reaction, the CYSMNPs were dispersed in ethanol absolute (Fisher Scientific, U.K.) and distilled water and the hydrolysis and polymerisation of tetraethyl ortosilicate (TEOS, Fluka Cheika, Germany) was favoured. Subsequently, as the reaction progressed and the TEOS hydrolysis and polymerisation processes neared completion, the polymerisation of resorcinol (Fisher Scientific, U.K.) and formaldehyde (37-38% p/p, Panreac, Spain) became the predominant process, resulting in the formation of a phenolic resin polymer layer[9]. To remove the Silica was used sodium hydroxide solution (Fisher Scientific, U.K.). The phosphate buffer solutions to drug loading and release were prepared with phosphate buffer solution (PBS, Fisher Scientific, USA), potassium dihydrogen phosphate (V.P., Portugal), disodium hydrogen phosphate 12-hydrate (Pronalab, Portugal), and sodium dihydrogen phosphate hydrate (Pronalab, Portugal).

3.2 Process fluxogram

For a better understanding of the process, the following fluxogram represents the steps of the methodology used, Figure 3. Those steps will be described in detail in sequence.

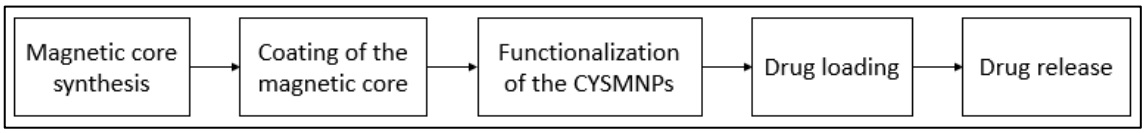

Figure 3 – Fluxogram of the process.

3.3 Magnetic core synthesis

The magnetic core was synthesized according to the methodology described by Awwad & Salem (2012), i.e., using a solution of Fe (II) and Fe (III). Approximately 0.53 g of $FeCl_2.4H_2O$ and 1.11 g of $FeCl_3.6H_2O$ (1:2 molar ratio) were dissolved in 100 mL of distilled water. The vessel containing this solution was placed in an oil bath on a magnetic stirring plate (IKA® C-MAG HS 7, Figure I - Annex A) with temperature control until 30 ºC (IKA® ETS-DS, Figure I - Annex A), and at this temperature, 5 mL of plant extract were added [6]. The extract concentration was 100 times higher than the EC 50 RP concentration, i.e. the extract concentration calculated from the method of Oyaizu (1986) to determine reducing power [60,61]. Different plant hydromethanolic extracts with high reducing power were investigated in the synthesis of magnetic cores, such as *Rubus ulmifolius* Schott flowers (EC 50 PR 40 $\mu g.mL^{-1}$), *Tamus communis L.* shoots (EC 50 PR 68 $\mu g.mL^{-1}$) and *Crateagus monogyna* Jacq. flowers (EC 50 PR 19 $\mu g.mL^{-1}$). After 5 minutes, 30 mL of ammonium hydroxide were added dropwise to the mixture using a peristaltic pump ISM 845, ISMATEC (Figure II - Annex A), Figure 4. The solution remained in stirring during 1 hour at 30 ºC. A representation of this synthesis methodology can be observed in Figure 5.

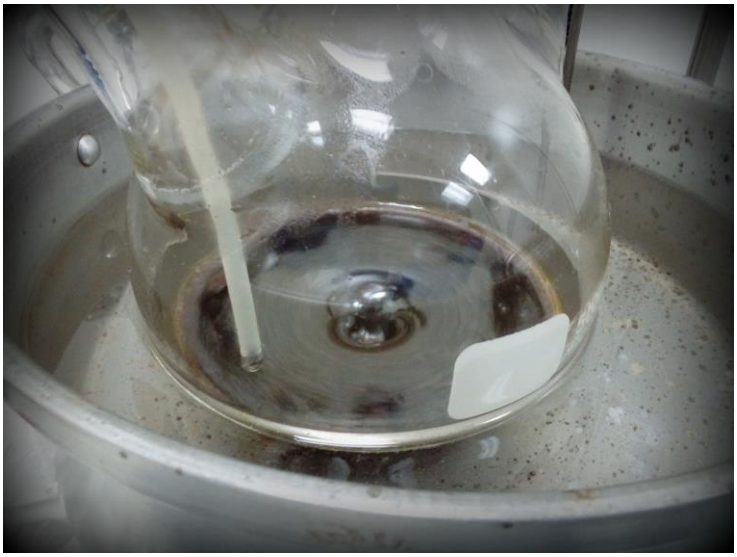

Figure 4 - Dropwise addition of ammonium hydroxide solution during the process of synthesis of the magnetic core.

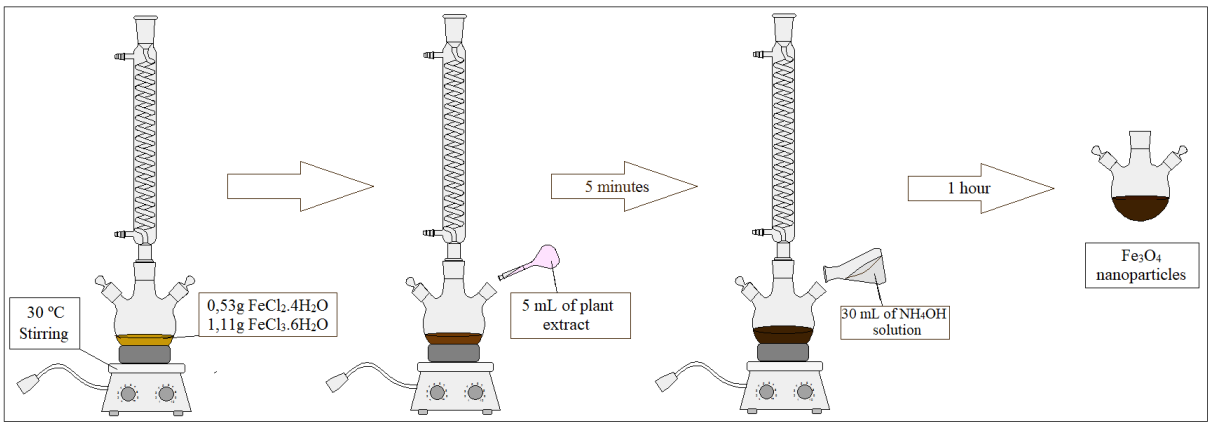

Figure 5 - Magnetic core synthesis methodology.

The solution was washed with distilled water by centrifugation at 600 rpm during 5 minutes in MPW-260R centrifuge, MPW Med. Instruments (Figure III - Annex A). The washing process was repeated 7 times. Finally, the last washing was done with ethanol and then the MNPs were dried at 60 ºC in a drying oven, Binder FD 115 (Figure IV - Annex A).

Subsequently, the magnetic core was characterized by X-ray diffraction (XRD) and Transmission Electron Microscopy (TEM) in order to perform phase identification and determine the crystalline structure and the total core size. XRD analysis was performed in a PANalytical X'Pert MPD equipped with a X'Celerator detector and secondary monochromator (Cu Kα λ= 0.154 nm; data recorded at a 0.017° step size). The composition of magnetite present were identified using HighScore software and Crystallography Open Database. Rietveld refinement of the XRD diffraction patterns was performed using PowderCell software allowing phase quantification. Crystallite sizes were determined by the Williamson-Hall method [62]. TEM was performed in a LEO 906E instrument operating at 120 kV, equipped with a 4 Mpixel 28 × 28 mm CCD camera from TRS [62]. ImageJ software was used to estimate the size of the magnetic nanoparticles.

3.2 Coating

The protocol proposed by Liu et. al. (2014) was used to produce the carbon-based coating. At the first step, 0.25 g of magnetic nanoparticles synthesized by the method previously described were suspended in 150 mL of ethanol and 50 mL of distilled water, which was ultrasonicated for 45 minutes, in Ultrasons-H, P-Selecta (Figure V - Annex A). That solution was then poured into a 500 mL round bottom flask with 0.05 g of resorcinol and 0.7 mL of ammonia solution (25%). That mixture remained in stirring for 1 h at 30 ºC in an oil bath on a magnetic stirring plate with temperature control. Then, 0.075 mL of formaldehyde solution (37-40%) and 0.100 mL of tetraethyl orthosilicate (TEOS) solution were added dropwise and the mixture stirred for 6 h at the same temperature. After that, the mixture was heated at 80 ºC for 8 h under stirring. The process was repeated with different reagent quantities, such as 0.1 g of resorcinol, 1.4 mL of ammonia solution (25%), 0.15 mL of formaldehyde solution (37-40%) and 0.205 mL of TEOS solution. The resultant solid was washed 7 times with distilled water by centrifugation at 600 rpm for 5 minutes. Finally, the last washing was done with ethanol absolute, then the MNPs were dried at 60ºC in the drying oven. The resultant NPs were denoted Fe_3O_4@polymer [9].

At the second step of the coating process, the Fe_3O_4@polymer sample was carbonized under a N_2 atmosphere in a vertical tubular furnace (ROS 50/250/12, Thermoconcept, Figure VI - Annex A). The carbonization occurred to 600 ºC at a heating rate of 1 ºC.min^{-1} and the temperature was maintained at 600 ºC for 3 h. The resultant NPs were denoted Fe_3O_4@SiO_2.C. Finally, the Fe_3O_4@SiO_2.C nanoparticles were etched under stirring with sodium hydroxide solution 10 mol.L^{-1} for 24 h at room temperature and the product was washed by centrifugation with distilled water several times, until reaching pH 7. After that, it was washed with ethanol and dried at 60 ºC in a drying oven. The obtained sample was Fe_3O_4@void@C [9]. The coated nanoparticles were characterized by TEM to determine the NPs total size and the carbon material thickness.

3.3 Functionalization

The functionalization of the CYSMNPs was performed by acid treatment. The coating product was added to nitric acid solution 1 $mol.L^{-1}$ in the ratio 5 mg:1 mL and maintained at 60 ºC for 1.5 h under stirring in oil bath on a magnetic stirring plate with temperature control. The process was repeated for other samples, but with time of reaction of 3 and 6 hours to compare the results. The product of the reaction was washed by centrifugation at 600 rpm during 5 minutes. The process was repeated several times with distilled water, and one more time with ethanol absolute, then the MNPs were dried at 60 ºC in a drying oven.

The samples were combined with KBr and compacted into pellets using a press in order to do analysis of spectra on Fourier transform infrared spectrometer (FT-IR). The analysis was performed for both non-functionalized and functionalized CYSMNPs in a ABB Inc. MB 3000 with a resolution of 16 cm^{-1} and a spectrum from 550 to 4000 cm^{-1}. The data was processed using Horizon MB 3.4 software allowing absorption bands identification.

The point of zero charge (pH_{pzc}) of the functionalized CYSMNPs were determined using NaCl solutions 0.01 M. Initially, 0.05 g of functionalized and non-functionalized CYSMNPs were placed in two different erlenmeyers and 20 mL of NaCl 0.01 M with pH initial of 7.22 (pH_i) were added in each erlenmeyer. After 48 hours in a IKA® KS 130 basic orbital shaker (Figure VII - Annex A), the mixtures were centrifuged 2 times at 6000 rpm during 5 minutes and the supernatant was used to measure the pH after their equilibration (pH_f). Subsequently, 0.05 g of non-functionalized CYSMNPs with 20 mL of NaCl 0.01 M pH_i 10.00 were placed in an erlenmeyer and 0.05 g of functionalized CYSMNPs with 20 mL of NaCl 0.01 M pHi 1.74 were placed in another erlenmeyer. The mixtures stayed in the orbital shaker during 48 hours and the centrifugation process was repeated, as well the measurement of pH_f. The comparison between pH_i and pH_f makes possible to establish the pH_{pzc} and to know the effect of functionalization in the nanocomposites.

3.4 Drug Loading and Release

Phosphate buffer solutions (PBS) with different pH were used for the tests with the drug. These solutions were prepared as following: a) PBS pH 4.5: 3.40 g of dihydrogen potassium phosphate was diluted in 0.5 L of distilled water; b) PBS pH 6.0: 49.2 mL of $Na_2HPO_4.12H_2O$ 0.2 M solution was mixed with 350.8 mL of $NaH_2PO_4.H_2O$ 0.2 M solution; c) PBS pH 7.4: the standard solution of PBS was diluted 10 times; d) PBS pH 8.0: 331.5 mL of $Na_2HPO_4.12H_2O$ 0.2 M solution was mixed with 18.5 mL of 0.2 M $NaH_2PO_4.H_2O$ solution.

First, a test was performed to analyze drug loading capacity (DLC) and drug loading efficiency (DLE) in different drug ratios for CYSMNPs. Solutions with the following concentrations of DOX were prepared in distilled water in 10 mL volumetric flasks: 20 $\mu g.mL^{-1}$, 50 $\mu g.mL^{-1}$, 100 $\mu g.mL^{-1}$, 200 $\mu g.mL^{-1}$, 400 $\mu g.mL^{-1}$ and 600 $\mu g.mL^{-1}$. The aspect of the DOX solutions can be observed in Figure 6. 1 mL of a DOX solution and 1 mL of CYSMNPs functionalized during 3 h were added in glass tubes, each concentration of DOX solution being analyzed in triplicate and the flasks protected from light. The samples stayed in the orbital shaker during 24 hours and after this time each sample was centrifuged 2 times in eppendorfs of 3 mL at 8000 rpm during 5 minutes. The supernatant was measured at 480 nm in a T70 UV-VIS spectrometer, PG Instruments Ltd. (Figure VIII - Annex A), to identify the concentration of the DOX that was loaded in each solution. The loading was expressed in terms of DLE and DLC. That test was repeated using DOX solutions in phosphate buffer solution (PBS) pH 7.4.

Figure 6 – Dox solutions of concentration 20 $\mu g.mL^{-1}$, 50 $\mu g.mL^{-1}$, 100 $\mu g.mL^{-1}$, 200 $\mu g.mL^{-1}$, 400 $\mu g.mL^{-1}$ and 600 $\mu g.mL^{-1}$, from left to right respectively.

To compare in which medium the drug load would be higher, different solutions were prepared with 5 mg of functionalized CYSMNPs during 3 and 6 h for a volume of 30

5 mL in different conditions: PBS pH 6.0, PBS pH 7.4 and PBS pH 8.0. Those solutions were mixed with 5 mL of Doxorubicin solution with a concentration of 1 $mg.mL^{-1}$ also prepared in PBS pH 6.0, PBS pH 7.4 and PBS pH 8.0. Those mixtures were placed in the orbital shaker for 24 h. Then, the samples were centrifuged and the supernatant was measured by UV-Vis spectrophotometry at 480 nm to determine the drug loading capacity. Subsequently, the solution which had better result was repeated in larger scale with 20 mg of functionalized CYSMNPs and 20 mg of Doxorubicin in 20 mL of solution, and after of the centrifugation, that sample was freeze-dried for the release test.

The release test was made in duplicate for different solutions: PBS pH 4.5, PBS pH 6.0 and PBS pH 7.4. Between 1 and 2 mg of freeze-dried CYSMNPs-DOX were weighed and 10 mL of each solution were added in each flask. The flasks were placed in the orbital shaker and after 30 minutes the mixture was centrifuged to separate CYSMNPs-DOX of the supernatant. The CYSMNPs-DOX returned for the flask, where 10 mL of the same solution were added and the flasks returned to the orbital shaker, while supernatant was measured by UV-Vis spectrophotometry at 480 nm to identify the concentration of the DOX that was released in each solution. This process of centrifugation and analysis of the supernatant was repeated in times of 1, 2, 4, 6, 24 and 48 h. From the data collected, a curve of the concentration released over time was plotted to analyze the difference of the drug release at different pH.

Chapter 4: Results and discussion

4.1 Synthesis of iron oxide nanoparticles

The synthesis of the magnetic cores were performed with the three plants extracts, *Rubus ulmifolius* Schott flowers, *Tamus communis L.* shoots and *Crateagus monogyna* Jacq. Flowers, which were compared among themselves. The three types of core were found to be very magnetic (Figure 7-a), to have black color and resulted in similar yields, approximately 516 mg, 501 mg and 416 mg, respectively (Figure 7-b). But visibly, the more stable magnetic core in distilled water was that synthesized with *Rubus ulmifolius* Schott flowers extract, as shown in Figure 8.

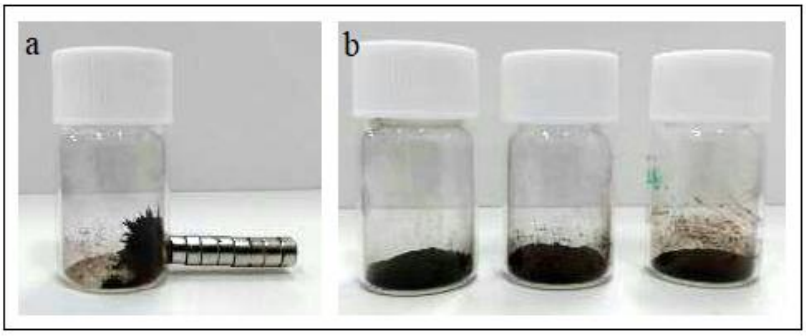

Figure 7 – a) Magnetic core; b) Magnetic cores synthesized with extracts of *Rubus ulmifolius* Schott flowers, *Tamus communis* L. shoots and *Crateagus monogyna* Jacq. flowers, from left to right respectively.

Figure 8 - Stability of the magnetic cores in distilled water with extracts of *Rubus ulmifolius* Schott flowers, *Tamus communis* L. shoots and *Crateagus monogyna* Jacq. flowers, from left to right respectively.

The XRD spectrum of the magnetic core nanoparticles are presented in Figure 9. The peaks at 30.62º, 35.75º, 43.37º, 53.70º, 57.38º, 63.06º and 74.37º are attributed to the crystal planes of the magnetic cores at 220, 311, 400, 422, 511, 440 and 533, respectively.

The relative intensity of the diffraction peaks match with the standard XRD data for magnetite (JCPDS no. 19-0629). Therefore, the investigation of phase by XRD confirms the crystal structure of the 3 cores synthesized as that of magnetite. Moreover, the core with *Rubus ulmifolius* Schott flowers extract has particle size of 13.5 ± 1 nm, while the cores with *Tamus communis* L. shoots and *Crateagus monogyna* Jacq. flowers extract have particle sizes of 12.3 ± 0.6 nm and 12.8 ± 0.5 nm, respectively. TEM image presented in Figure 10 shows magnetite core synthesized with *Rubus ulmifolius* Schott flowers extract with average size of 13.42 ± 3.51 nm. The observed agglomeration is related to the magnetic characteristics of the sample.

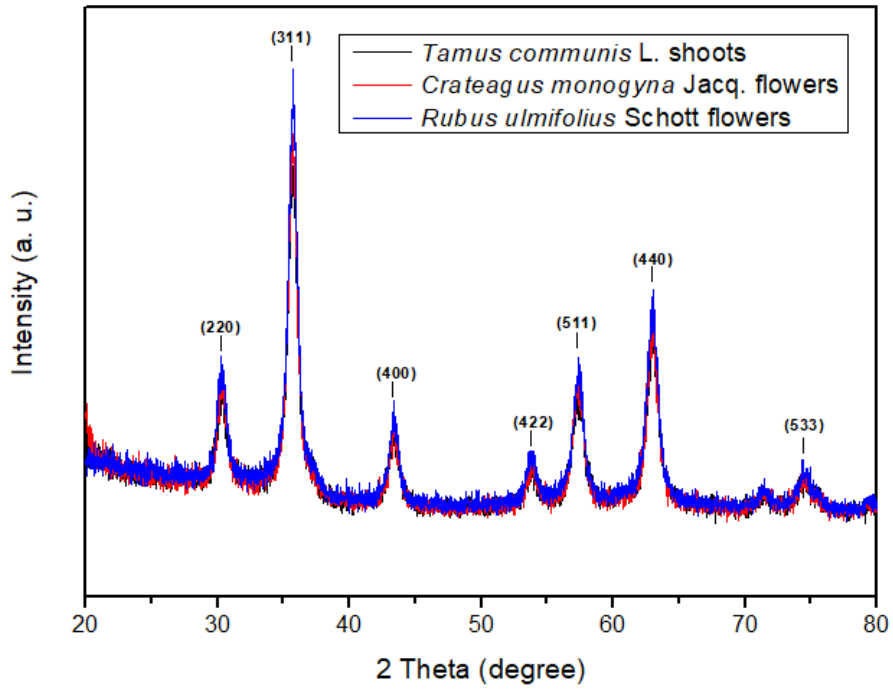

Figure 9 - XRD patterns of the magnetic cores synthesized with *Rubus ulmifolius* Schott flowers, *Tamus communis* L. shoots and *Crateagus monogyna* Jacq. flowers extracts.

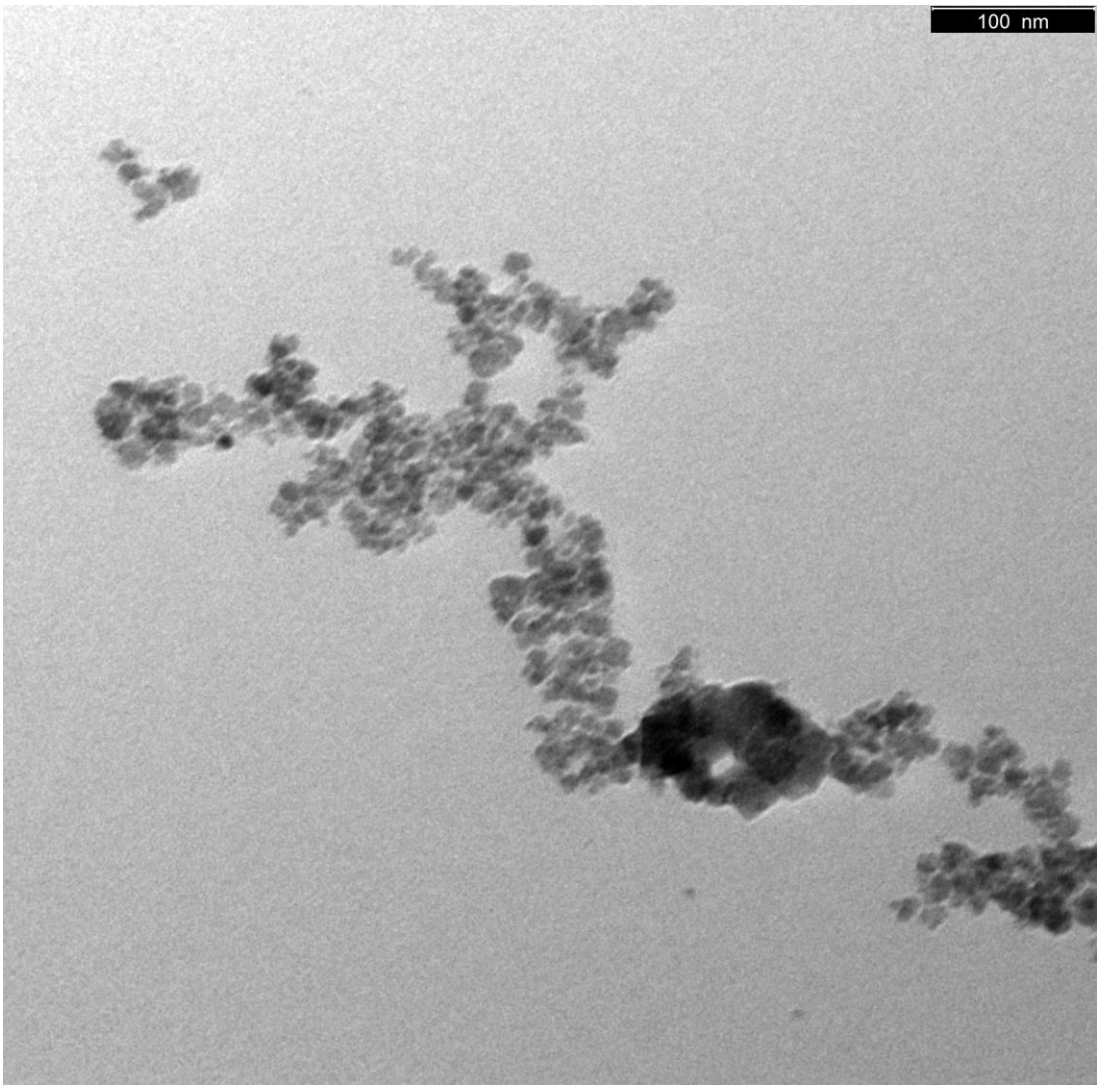

Figure 10 - TEM image of the magnetite core synthesized with *Rubus ulmifolius* Schott flowers extract.

Because of the best stability in distilled water of the magnetic core produced with the *Rubus ulmifolius* Schott flowers extract, this was chosen to continue the experiments. That species, known as wild blackberry, is regarded as an interesting medicinal plant and considered to be anti-catarrhal, antiseptic, diuretic, anti-inflammatory, antioxidant, astringent and antispasmodic. In its extract, twenty-four phenolic compounds can be identified, such as phenolic acid derivatives (di- and caffeoylquinic, p-coumaroylquinic, feruloylquinic acids and ellagic acid), flavonoids (quercetin and kaempferol derivatives and catechin) and hydrolysable tannins (lambertianin, sanguiin and four di-hexahydroxydiphenol (HHDP)- galloyl glucose isomers) [60]. For the green routes synthesis, the flavonoids are probably involved in the stages of initiation of nanoparticle formation and further aggregation, in addition to the bioreduction stage, because they

contain various functional groups capable of nanoparticle formation [44]. Besides the composition and reducing power of the extract, the methodology adopted uses ammonium hydroxide to perform the synthesis of the magnetite core by the chemical precipitation method.

4.2 Carbon-based coating

The coating processes of the magnetite core were identified according to the quantities of reagents used, as follows: a) 0.05 g of resorcinol, 0.7 mL of ammonia solution (25%), 0.075 mL of formaldehyde solution (37-40%) and 0.100 mL of TEOS solution; and b) 0.1 g of resorcinol, 1.4 mL of ammonia solution (25%), 0.15 mL of formaldehyde solution (37-40%) and 0.205 mL of TEOS solution. It was found that the coating process ‘a’ was not sufficient to cover the magnetite core. In addition, during this process, the magnetite nanoparticle was oxidized and the resulting solid had a dark red appearance. However, the coating process ‘b’ resulted in coated nanoparticles of dark black color and preserved the initial magnetic characteristics. Both samples were analyzed by TEM (Figure 11), which made possible to know the size of the coated nanoparticles. The coating processes ‘a’ and ‘b’ resulted in particles with average sizes of 12.99 ± 3.29 nm and 20.16 ± 8.68 nm, respectively.

When the objective is to have a material for drug delivery application, there is a need for better therapeutic materials that have good drug solubility, an ability to reduce systemic toxicity through specific-tumor targeting and rapid clearance[63]. Carbon-based nanomaterials are important due to their unique combination of chemical and physical properties, such as thermal and electrical conductivity, high mechanical strength and optical properties, then higher chemical and thermal stability, larger surface area, biocompatibility and easier functionalization. Due to those advantageous properties they are also actively investigated in several areas of biomedical engineering [63,64].

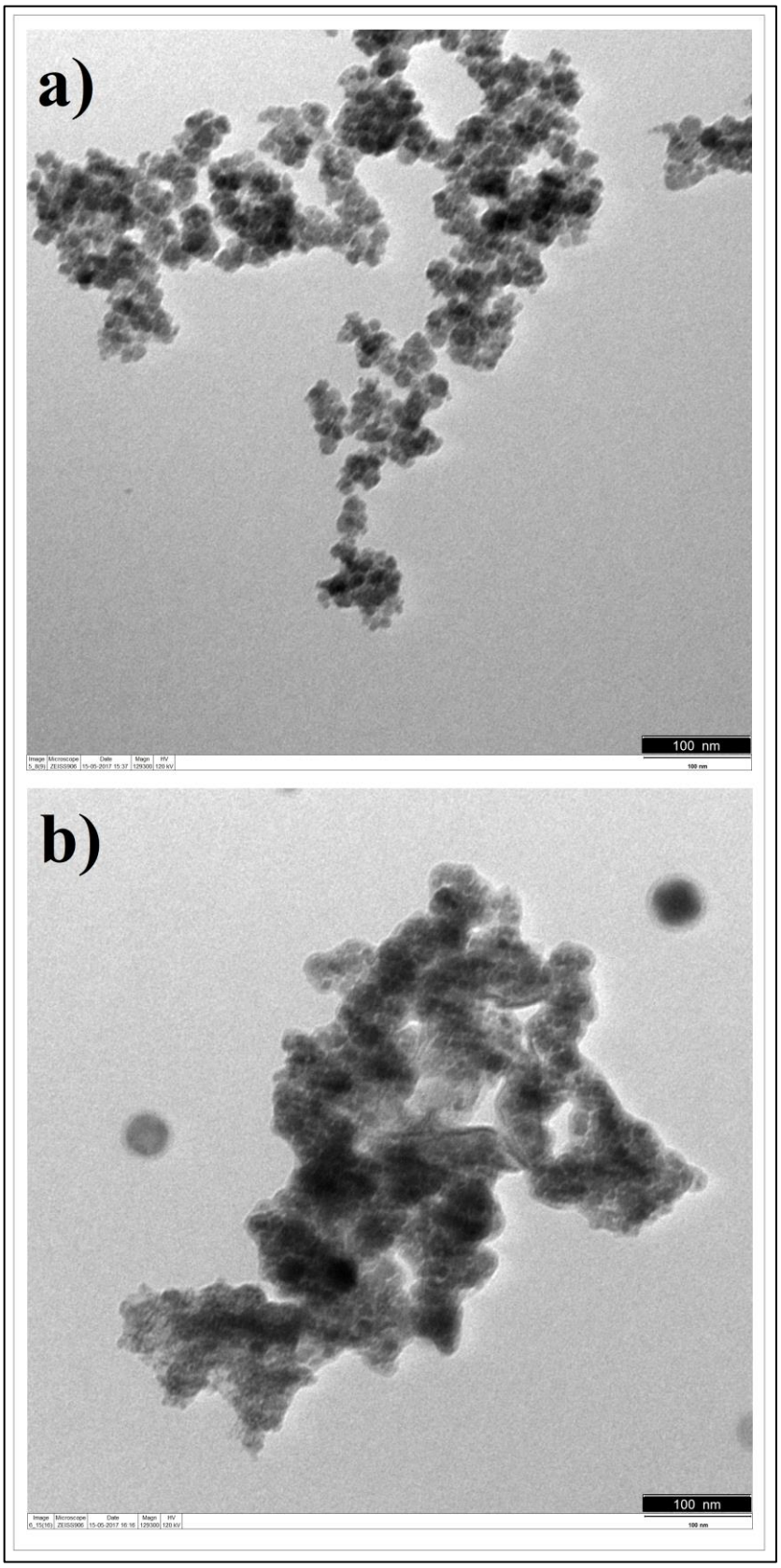

Figure 11 - TEM images of the samples resulted from the coating processes ‘a’ and ‘b’, from left to right respectively.

According to Liu *et. al.* (2014), the magnetic mesoporous carbon hollow nanoparticles can be used as drug delivery carriers and diagnostic agents for cancer, due to the large volume in the cavity between the yolk and the shell that provides sufficient space for the loading of drugs. Moreover, the use of magnetic nanocomposites with a YS mesoporous structure can be an effective solution to CS structure problem; since the CS magnetic properties are sometimes restrained to a specific range because the core materials are easily and compactly encapsulated in the shell material, while YS materials with interstitial spaces between the mesoporous shells and the magnetic cores can have movable magnetic nanoparticles packed in the mesoporous hollow shells [9]. However, it has been confirmed that the nanoparticles coated by process 'b' have sufficient space for higher drug loading capacity, as will be seen below.

4.3 The effects of the functionalization

The functionalization with nitric acid added carboxylic acid groups (-COOH) to the CYSMNPs structures, increasing the acidity of the nanocomposites. The point of zero charge (pH_{pzc}) was investigated to compare the acidity of the material before and after functionalization, with the measures of pH_i and pH_f the graphs 12-a and 12-b were constructed, Figure 12.

From the equation of the line obtained by the graph, knowing that it represents the pH_f and that the zero load point is found by means of the chemical equilibrium, when we consider pH_i=pH_f, the pH_{pzc} value is found using the following equations:

$$y = 0{,}2878x + 6{,}5823 \quad \text{(a)}$$

$$y = 0{,}292x + 1{,}352 \quad \text{(b)}$$

If pH_i=pH_f, so y=x. These values of x and y correspond to 9.24 and 1.91 for the non-functionalized (12-a) and functionalized (12-b) CYSMNPs, respectively. Those results showed that functionalization made the CYSMNPs more acidic.

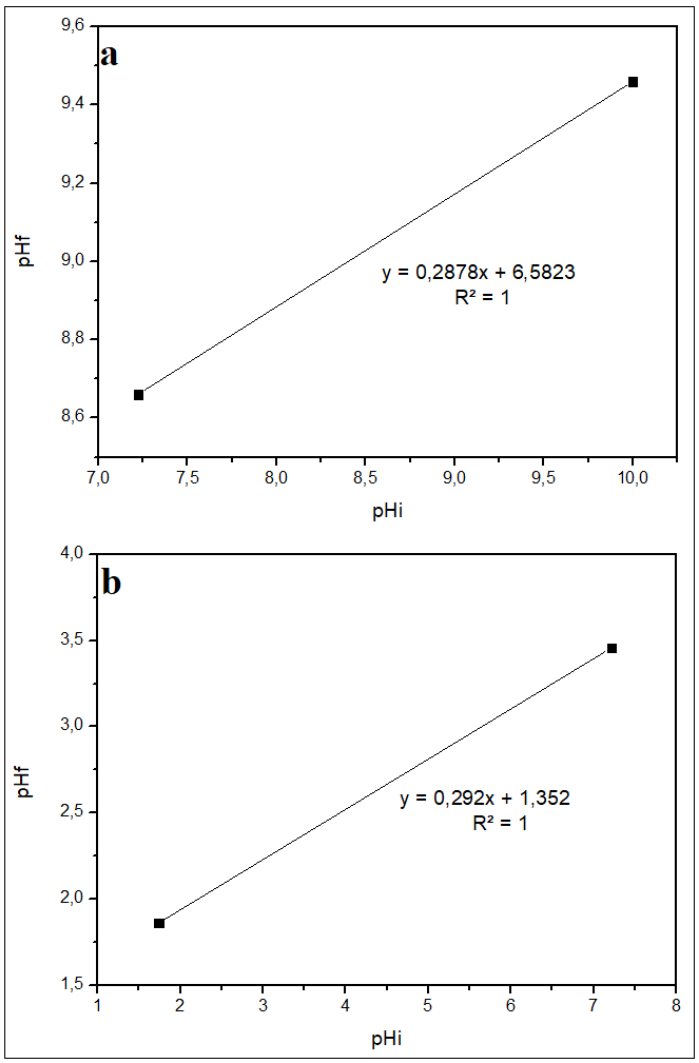

Figure 12 – Results of measurement of pH_i and pH_f resulting from the pHpzc test of a) non-functionalized CYSMNPs; and b) functionalized CYSMNPs.

In addition, the spectral analysis in the Fourier transform infrared spectrometer (FT-IR), Figure 13, shows the comparison of the spectra of the nanocomposites before and after functionalization. The presence of magnetite in non-functionalized CYMNPs is noticed in the absorption bands of 564 cm^{-1}, 1628 cm^{-1} and 3433 cm^{-1}. The first band corresponds to the vibration of the Fe–O bond, and the latter two can be attributed to the bending and stretching vibrations of the surface –OH groups present in Fe_3O_4 [65].

The absorption bands at 1380 cm^{-1}, 1458 cm^{-1}, 1627 cm^{-1}, 2923 cm^{-1} and 3433 cm^{-1} represent the C-O, O-H, C=O, C-H and O-H bonds respectively, which indicate that there are carboxylic acid groups in the samples. In the functionalized sample the increase in the absorption band in the region 1000-1400 cm^{-1} can be attributed to the C-O stretching frequencies of the -COOH groups [65]. In addition, the increase in the intensity

of the absorption bands at 1380 and 1627 cm^{-1} represents the increase in the C-O and C=O bonds of the carboxylic acid groups [66]. However, this indicates the increase of the carboxyls, which are responsible for making the nanocomposites more acidic. The presence of carboxyls in nanocomposites can improve colloidal stability and monodispersibility in aqueous solutions [66].

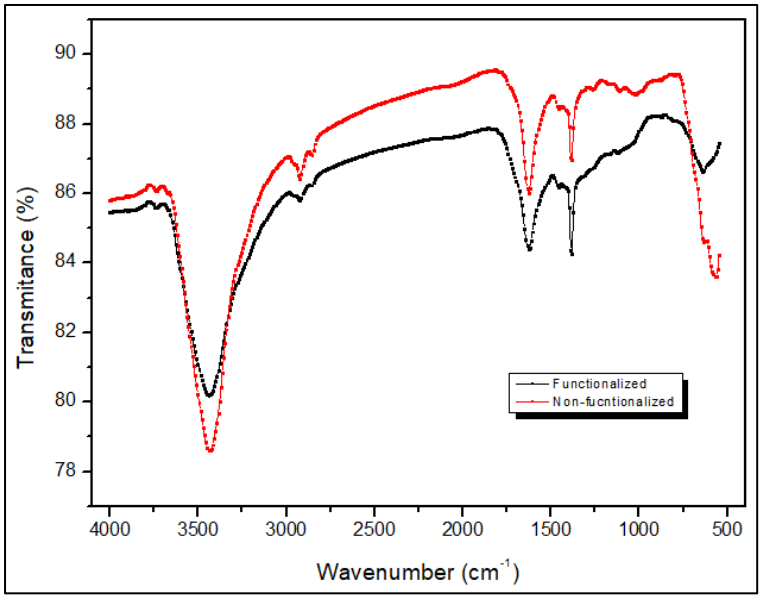

Figure 13 - Absorption bands of functionalized and non-functionalized CYSMNPs.

4.4 Capacity and efficiency of drug loading

Initially, the DLC ($\mu g.\mu g^{-1}$) and DLE (%) were studied for solutions with different concentrations of DOX in 2 solution media (distilled water and PBS pH 7.4) using functionalized CYSMNPs during 3 hours.

$$DLC = \frac{C_{DOX-CYSMNPs}}{C_{CYSMNPs}} \quad (1)$$

$$DLE(\%) = \frac{C_{0DOX} - C_{fDOX}}{C_{0DOX}} * 100 \quad (2)$$

Where, $C_{DOX\text{-}CYSMNPs}$ is concentration of Doxorubicin loaded in the CYSMNPs, $C_{CYSMNPs}$ is concentration of CYSMNPs, C_{0DOX} is initial concentration of DOX before loading, $C_{f\,DOX}$ is final concentration of DOX in supernatant after loading.

The results of this test can be observed in Figure 14. The DLC and DLE maximum were 0.193 $\mu g.\mu g^{-1}$ (300 $\mu g_{DOX}.mL^{-1}$) and 97.9 % (50 $\mu g_{DOX}.mL^{-1}$) for solutions in distilled water, and 0.514 $\mu g.\mu g^{-1}$ (300 $\mu g_{DOX}.mL^{-1}$) and 98.4% (100 $\mu g_{DOX}.mL^{-1}$) for solutions in PBS pH 7.4. Therefore, PBS pH 7.4 is better than distilled water to be used as the loading medium. In addition to the electrolytes present in distilled water that do not allow its pH to remain constant, the solution whose pH is closest to pKa of the drug (Doxorubicin, pKa 8.3) will have better absorption of it.

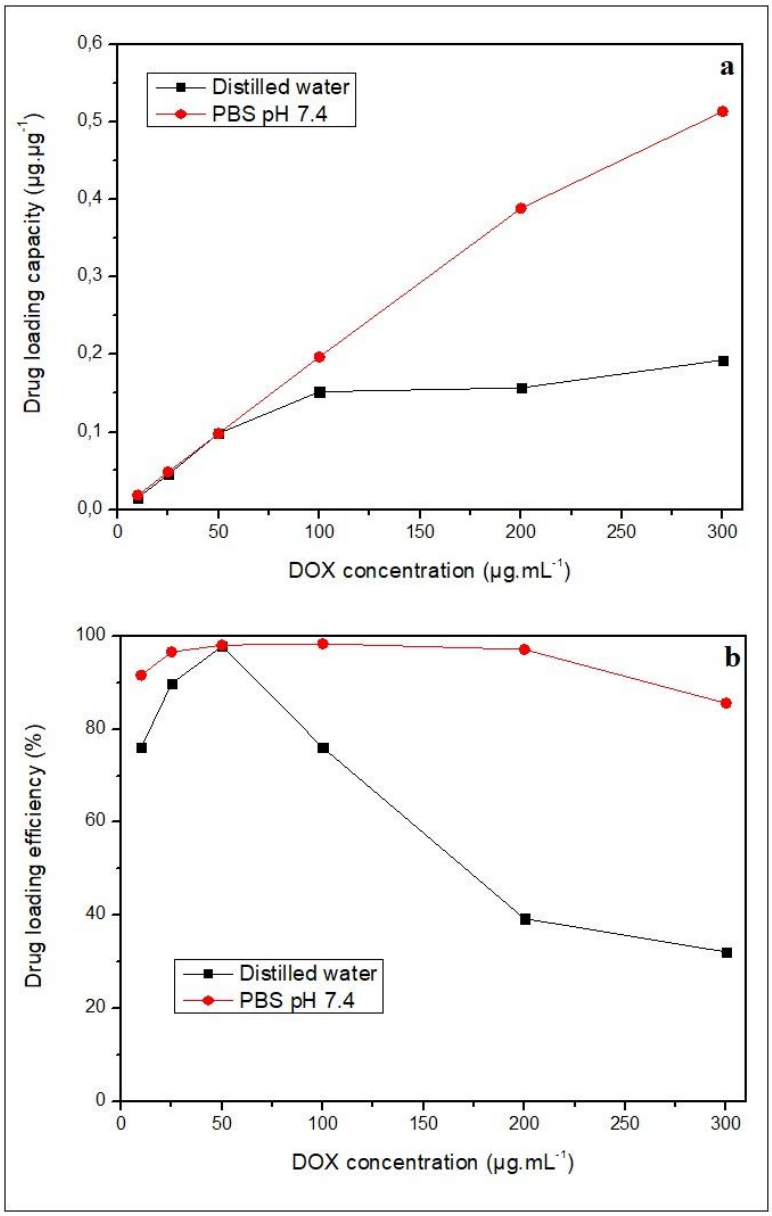

Figure 14 – Results of drug loading test in distilled water and PBS pH 7.4. a) Drug loading capacity; b) Drug loading efficiency.

After this initial test of drug loading, a test with CYSMNPs functionalized for 3 and 6 h was compared in other PBS solutions with different pH. The ratio of drug and CYSMNPs used for this comparison test was 1:1 (w/w). Figure 15 shows the solutions prepared that were used in this test, and Figure 16 shows the supernatants of those samples after centrifugation and separation of the nanoparticles. The DLC and DLE values are given in Table 1.

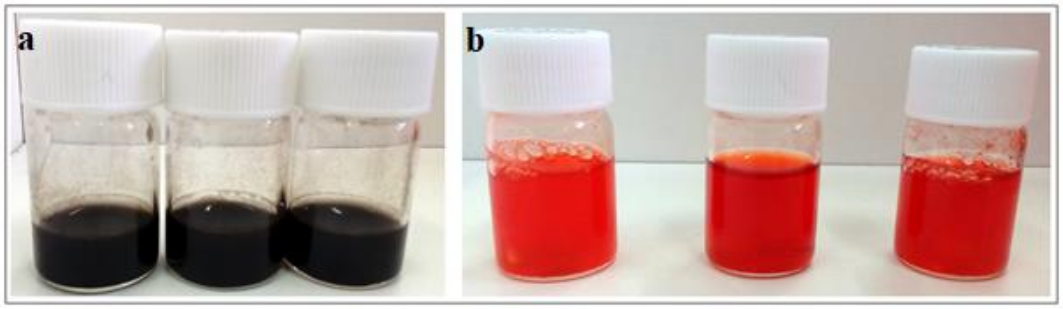

Figure 15 - a) Functionalized CYSMNP in solutions of pH 6.0, pH 7.4 and pH 8.0, from left to right respectively; b) Doxorubicin in solutions of pH 6.0, pH 7.4 and pH 8.0, from left to right respectively.

Figure 16 - The samples of supernatants used to analyze drug loading efficiency and drug loading capacity in different pH by UV-Vis at 480 nm (The samples above correspond to pH 6.0, pH 7.4 and pH 8.0, from left to right respectively).

Table 1 – Results of drug loading test with different functionalization times in different solutions.

Solutions	Functionalization 3 h		Functionalization 6 h	
	DLC ($\mu g.\mu g^{-1}$)	DLE (%)	DLC ($\mu g.\mu g^{-1}$)	DLE (%)
PBS pH 6.0	0.934 ± 0.007	93.4 ± 0.7	0.943 ± 0.005	94.3 ± 0.5
PBS pH 7.4	0.955 ± 0.004	95.5 ± 0.4	0.981 ± 0.001	98.1 ± 0.1
PBS pH 8.0	0.996 ± 0.000	99.6 ± 0.0	0.996 ± 0.001	99.6 ± 0.1

The loading difference at different pH can be explained mainly due to the solution whose pH is approximately the pKa of the drug (Doxorubicin, pKa 8.3). As explained previously, this allows greater electrostatic affinity between the drug (positively charged) and the functionalized CYSMNPs (negatively charged), and consequently a higher drug loading.

Although stability in aqueous solution had increased with the functionalization during 6 h, it also affected the magnetic characteristics of CYSMNPs. Therefore, and also because these nanoparticles did not present significant differences in drug loading, it was decided to continue the experiments only with the functionalization of 3 h. In addition, functionalizing for 3 h saves time and has a better recovery of the material during the washings of the solids resulting from the reaction. Then, the two best results for CYSMNPs functionalized during 3 h (PBS 7.4 and PBS 8.0) were repeated with more quantity, 20 mg of functionalized CYSMNPs, to prepare samples for drug release. The results are shown in Table 2.

Table 2 - Results of drug loading to prepare samples for drug release.

Solutions	Functionalization 3 h	
	DLC ($\mu g.\mu g^{-1}$)	DLE (%)
PBS pH 7.4	0.914	91.4
PBS pH 8.0	0.993	99.3

It is noteworthy that increasing the mass for the same process, the values of DLC and DLE decreased. Even though the result for the PBS solution at pH 8.0 was better, during the process of preparing the solutions for loading, it was observed that in this medium the drug had poor solubility. Therefore, even though the solution of pH 7.4 did not have the best results, they would be more reliable, besides having a better drug solubility. So, CYSMNPs-DOX loaded at pH 7.4 was chosen to perform the release tests.

4.5 pH dependent release

The pH dependent release is very important due to the difference between the pH of the normal tissues (pH 7.4), the extracellular environment of the tumor (pH 6.5) and

the endosome and lysosome (pH 5.0) [56]. Therefore, if more drug is released in the more acidic environment, the better will be the treatment of the tumor and lower will be the side effects and damage to the healthy cells. The release test previously described presented higher drug release in acidic medium, as expected. The cumulative drug release (%) of the amount of drug retained in nanocomposites were 32.35%, 27.18% and 11.95% in PBS solutions with pH 4.5, pH 6.0 and pH 7.5, respectively, Figure 17. These results can be expressed in cumulative concentration 52.01 $\mu g.ml^{-1}$, 37.26 $\mu g.ml^{-1}$ and 16.39 $\mu g.ml^{-1}$, which represent in weight of DOX the quantities of 520.16 µg, 372.56 µg and 163.86 µg in PBS solutions with pH 4.5, pH 6.0 and pH 7.5, respectively. The drug release over time is represented in Figure 18.

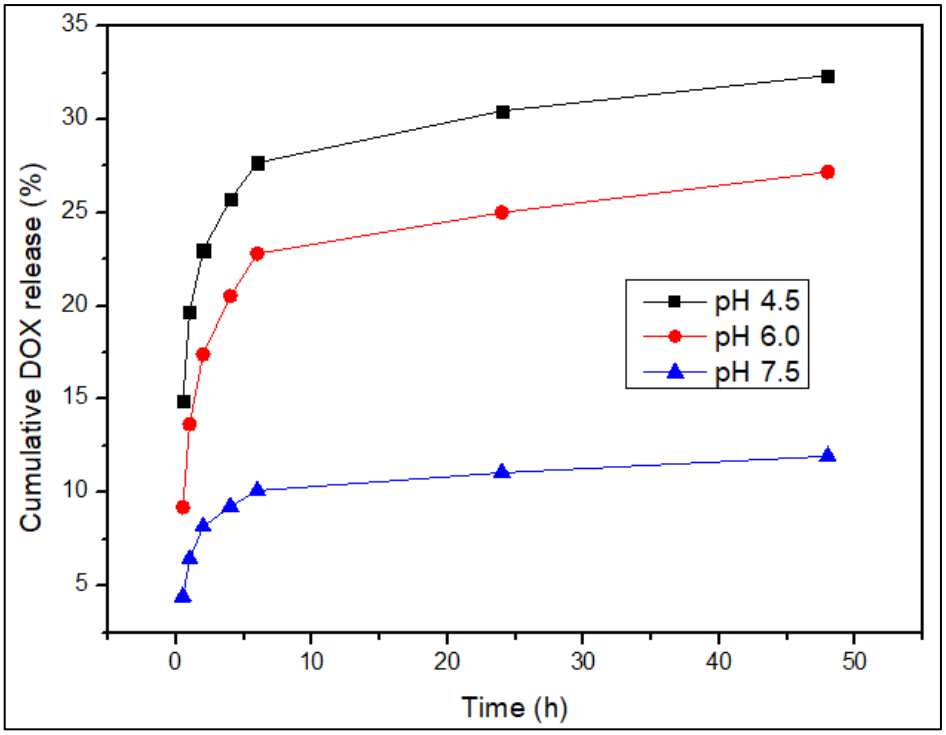

Figure 17 - Drug release in percentage of DOX over time.

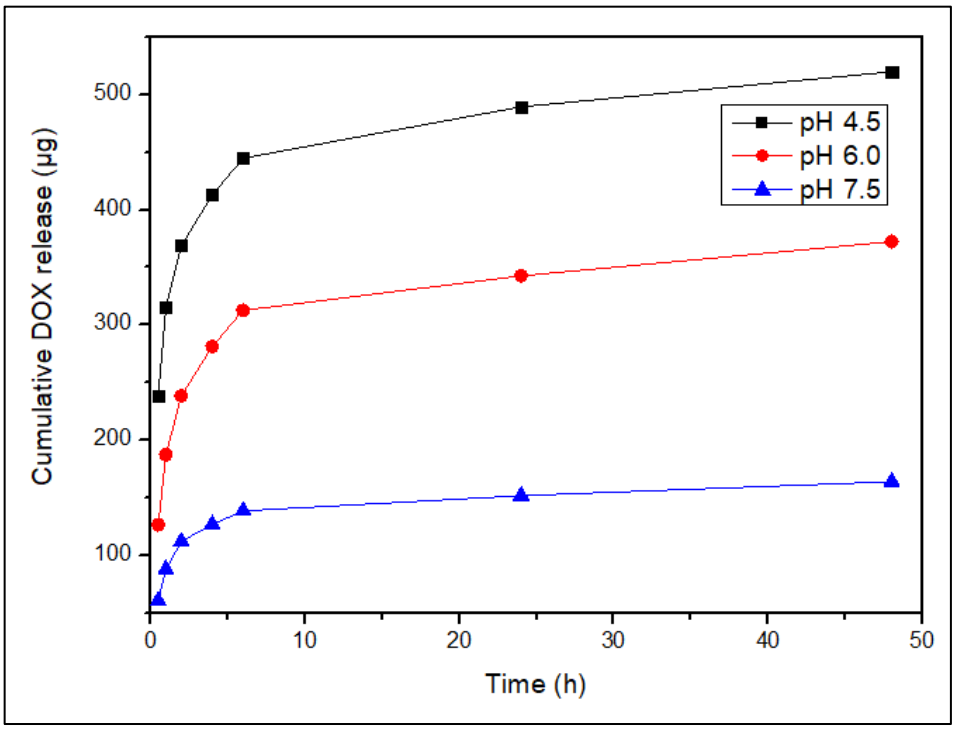

Figure 18 – Drug release in weight of DOX over time.

The drug release has shown to have a dependence with the pH of the targeting cells with acid pH. Thus, pH controlled drug release would be a viable application to the synthesized material. The CYSMNs would be conducted to the target with a magnetic field and the pH of the environment would act on the release of the drug. The disadvantage is that much weight of the drug was retained in the CYSMNPs, but the amount released is still relevant to the application for which it is proposed. Therefore, this research demonstrates the outstanding ability to use the developed and optimized green CYSMNPs, as super-drug nanocarriers with great ability to load high content of the anticancer drug Doxorubicin.

Chapter 5: Conclusions and future research

5.1 Conclusions

Based on the premise of optimizing yolk-shell magnetic nanocomposites for the treatment of cancer, this thesis was concluded aiming to obtain the release of higher amount of drug in the more acidic medium, which corresponds to the medium of cancer cells. Thus, considering all the optimizations made during the synthesis, coating, functionalization and loading and release of the drug, the final release result obtained was approximately 20% higher in solution with equivalent pH to the cancer cells than in an in solution with equivalent pH to normal cells. A considerable disadvantage was the large amount of drug retained in the material, which still needs an optimization to improve the drug exploitation and to obtain better yield of release. Therefore, in this study, the synthesized nanocomposites CYSMNPs were efficient and intelligent for application in targeted drug delivery.

5.2 Future research

A hyperthermia study will be conducted to apply these nanocomposites synergistically for drug administration and hyperthermia, thinking about a more effective treatment of cancer. In addition, drug release needs to be improved so that fewer drugs are maintained in the nanocomposites. There is interest in performing other tests such as the zeta potential to determine the surface charge of nanoparticles in solution (colloids), among others tests and optimization to assess the viability of applying this material both for its capacity and harmlessness.

Chapter 6: References

1. Teja A.S., Koh P. (2009). Synthesis, properties, and applications of magnetic iron oxide nanoparticles. Progress in Crystal Growth and Characterization of Materials 55: 22–45.

2. Mohapatra S., Rout S. R., Das R. K., Nayak S., Ghosh S. K. (2016). Highly hydrophilic luminescent magnetic mesoporous carbon nanospheres for controlled release of anticancer drug and multimodal imaging. Langmuir 32: 1611–1620.

3. Sun C., Lee J.S.H., Zhang M. (2008). Magnetic nanoparticles in MR imaging and drug delivery. Advanced Drug Delivery Reviews 60: 1252–1265.

4. Zamora-Mora V., Fernández-Gutiérrez M., González-Gómez A., Sanz B., Román J.S., Goya G.R., Hernández R., MIjangos C. (2017). Chitosan nanoparticles for combined drug delivery and magnetic hyperthermia: from preparation to in vitro studies. Carbohydrate Polymers 157: 361–370.

5. Faraji M., Yamini Y., Rezaee M. (2010). Magnetic nanoparticles: synthesis, stabilization, functionalization, characterization and applications. Journal of the Iranian Chemical Society 7: 1–37.

6. Awwad A. M., Salem N. M. (2012). A green and facile approach for synthesis of magnetite nanoparticles. Journal of Nanoscience and Nanotechnology 2: 208–213.

7. Shah S., Dasgupta S., Chakraborty M., Vadakkekara R., M. H. (2012). Green synthesis of iron nanoparticles using plant extracts. International Journal of Biological & Pharmaceutical Research 3: 767–774.

8. Yew Y. P., Shameli K., Miyake M., Kuwano N., Khairudin N. B. Bt A., Mohamad S. E. Bt, Lee K. X. (2014). Green synthesis of magnetite (Fe3O4) nanoparticles using seaweed (Kappaphycus alvarezii) extract. Nanoscale Research Letters 11:276.

9. Liu W., Liu Y.,Yan X., Young G., Xub Y., Liu S. (2014). One-pot synthesis of yolk-shell mesoporous carbon spheres with high magnetisation. Journal of Materials Chemistry A 2: 9600–9606.

10. Munnier E., Cohen-Jonathana S., Linassier C., Douziech-Eyrollesa L., Marchaisa H., Soucé M., Hervé K., Dubois P., Chourpa I. (2008). Novel method of doxorubicin-SPION reversible association for magnetic drug targeting. International Journal of Pharmaceutics 363: 170–176.

11. Munnier E., Cohen-Jonathana S., Hervéa K., Linassier C., Soucé M., Dubois P., Chourpa I. (2011). Doxorubicin delivered to MCF-7 cancer cells by superparamagnetic iron oxide nanoparticles: effects on subcellular distribution and cytotoxicity. Journal of Nanoparticle Research 13: 959–971.

12. Francisquini E., Schoenmaker J., Souza J. A. (2014). Nanopartículas magnéticas e suas aplicações. Química Supramolecular e Nanotecnologia. Chapter 4.

13. Nanotechnology Definition. Available at: http://www.understandingnano.com/nanotechnology-definition.html. (Accessed: 22nd January 2017).

14. Magnetic nanoparticles: nanomagnetic-project. Available at: http://www.nanomag-project.eu/magnetic-nanoparticles.html. (Accessed: 22nd January 2017).

15. Swihart M. A. (2007). Magnetic Materials. Control 1–6816.

16. Parker J. R. (1989). The variations of magnetic behavior. Advances in permanente magnetism. Wiley. Chapter 3: 44-46.

17. Ramanujan R. V. (2013) Magnetic particles for biomedical applications. Biomedical Materials. Chapter 17: 477–491.

18. Tietze R., Zaloga J., Unterweger H., Lyer S., Friedrich R. P., Janko C., Pöttler M., Dürr S., Alexiou C. (2015). Magnetic nanoparticle-based drug delivery for cancer therapy. Biochemical and Biophysical Research Communications. 468:463–470.

19. Arruebo M., Fernández-pacheco R., Ibarra M. R., Santamaría J. (2007). Magnetic nanoparticles controlled release of drugs from nanostructured functional materials. Nano Today Journal. 2: 22–32.

20. Behrens S., Appel I. (2016). Magnetic nanocomposites. Current Opinion in Biotechnology 39: 89–96.

21. Beygi H., Babakhani A. (2017). Microemulsion synthesis and magnetic properties of FexNi(1-x) alloy nanoparticles. Journal of Magnetism and Magnetic Materials. 421: 177–183.

22. Capek I. (2004). Preparation of metal nanoparticles in water-in-oil (wyo) microemulsions. Advances in Colloid and Interface Science 110: 49–74.

23. Roca A. G., Morales P., O'Grady K., Serna C.J. (2006). Structural and magnetic properties of uniform magnetite nanoparticles prepared by high temperature decomposition of organic precursors. Nanotechnology 17:2783–2788.

24. Demazeau G. (2001). Solvothermal and hydrothermal processes: the main physico-chemical factors involved and new trends. Research on Chemical Intermediates 37:107–123.

25. Zhang W., Shen F., Hong R. (2011). Solvothermal synthesis of magnetic Fe3O4 microparticles via self-assembly of Fe3O4 nanoparticles. Particuology 9: 179–186.

26. Yan A., Liu X., Qiu G., Wu H., Yi R., Zhang N., Xu J. (2008). Solvothermal synthesis and characterization of size-controlled Fe3O4 nanoparticles. Journal of Alloys and Compounds 458: 487–491

27. Zhu S., Guo J., Dong J.,Cui Z., Lu T., Zhu C., Zhang D., Ma J. (2013). Sonochemical fabrication of Fe3O4 nanoparticles on reduced graphene oxide for biosensors. Ultrasonics sonochemistry 20: 872–880.

28. Suslick K. S., Didenko Y., Fang M.M., Hyeon T., Kolbeck K.J., McNamara III W.B., Mdleleni M.M., Wong M. (1999). Acoustic cavitation and its chemical consequences. Philosophical Transactions of the Royal Society of London 357: 335–353.

29. Kim E. H., Lee H. S., Kwak B. K., Kim B. K. (2005) Synthesis of ferrofluid with magnetic nanoparticles by sonochemical method for MRI contrast agent. Journal of Magnetism and Magnetic Materials 289: 328–330.

30. Carenza E., Barceló V., Morancho A., Montaner J., Rosell A., Roig A. (2014). Rapid synthesis of water-dispersible superparamagnetic iron oxide nanoparticles by a microwave-assisted route for safe labeling of endothelial progenitor cells. Acta Biomaterialia 10: 3775–3785.

31. Hugh O. Pierson. (1992). Handbook of chemical vapor deposition: principles, technology and applications. Noyes publications.

32. Huang M., Qin M.,Cao Z., Jia B., Chena P., Wu H., Wang X., Wan Q., Qu X. (2016). Magnetic iron nanoparticles prepared by solution combustion synthesis and hydrogen reduction. Chemical Physics Letters 657: 33–38

33. Safari A., Gheisari K., Farbod M. (2017). Characterization of Ni ferrites powders prepared by plasma arc discharge process. Journal of Magnetism and Magnetic Materials 421: 44–51.

34. Dumitrache F., Morjan I., Alexandrescu R., Ciupina V., Prodan G., Voicu I., Fleaca C., Albu L., Savoiu M., Sandu I., Popovici E., Soare I. (2005). Iron-iron oxide core-shell nanoparticles synthesized by laser pyrolysis followed by superficial oxidation. Applied Surface Science 247: 25–31.

35. Alexandrescu R., Morjan I., Dumitrache F., Birjega R., Jaeger C., Mutschke H., Soare I., Gavrila-Florescu L., Ciupina V. (2007). Structural characteristics of Fe3C-based nanomaterials prepared by laser pyrolysis from different gas-phase precursors. Materials Science and Engineering C 27: 1181–1184.

36. Hong R. Y., Li J.H., Li H.Z., Ding J., Zheng Y., Wei D.G. (2008). Synthesis of Fe3O4 nanoparticles without inert gas protection used as precursors of magnetic fluids. Journal of Magnetism and Magnetic Materials. 320: 1605–1614.

37. Harshiny M., Iswarya C. N., Matheswaran M. (2015). Biogenic synthesis of iron nanoparticles using Amaranthus dubius leaf extract as a reducing agent. Powder Technology 286: 744–749.

38. Wang Z., Fang C., Mallavarapu M. (2015). Characterization of iron-polyphenol complex nanoparticles synthesized by Sage (Salvia officinalis) leaves. Environmental Technology & Innovation 4: 92–97.

39. Makarov V. V., Makarova S. S., Love A. J., Sinitsyna O. V., Dudnik A. O., Yaminsky I. V., Taliansky M. E., Kalinina N. O. (2014). Biosynthesis of Stable Iron Oxide Nanoparticles in Aqueous Extracts of Hordeum vulgare and Rumex acetosa Plants. Langmuir 30: 5982–5988.

40. Martínez-Cabanas M., López-García M., Barriada J. L., Herrero R., Sastre de Vicente, M. E. (2016). Green synthesis of iron oxide nanoparticles. Development of magnetic hybrid materials for efficient As(V) removal. Chemical Engineering Journal 301: 83–91.

41. Prasad C., Gangadhara S., Venkateswarlu P. (2015). Bio-inspired green synthesis of Fe3O4 magnetic nanoparticles using watermelon rinds and their catalytic activity. Applied Nanoscience 6: 797–802.

42. Wang T., Lin J., Chen Z., Megharaj M., Naidu R. (2014). Green synthesized iron nanoparticles by green tea and eucalyptus leaves extracts used for removal of nitrate in aqueous solution. Journal of Cleaner Production 83: 413–419.

43. Wu Y., Zeng S., WangaF., Megharaj M., Naidu R., Chen Z. (2015). Heterogeneous Fenton-like oxidation of malachite green by iron-based nanoparticles synthesized by tea extract as a catalyst. Separation and Purification Technology 154: 161–167.

44. Makarov V. V., Love A. J., Sinitsyna O. V., Makarova S. S., Yaminsky I. V., Taliansky M. E., Kalinina N. O. (2014). Green nanotechnologies: synthesis of metal nanoparticles using plants. Acta Naturae 6: 35–44.

45. Machado S., Pacheco J. G., Nouws H. P. A., Albergaria J. T., Delerue-Matos C. (2015). Characterization of green zero-valent iron nanoparticles produced with tree leaf extracts. Science of the Total Environment 533: 76–81.

46. Mahdavi M., Namvar F., Ahmad M. B., Mohamad R. (2013). Green biosynthesis and characterization of magnetic iron oxide (Fe_3O_4) nanoparticles using seaweed (Sargassum muticum) aqueous extract. Molecules 18: 5954–5964.

47. Al-kalifawi E. J. (2015). Green synthesis of magnetite iron oxide nanoparticles by using Al-Abbas's (A.S.) hund fruit (Citrus medica) var. Sarcodactylis Swingle extract and used in Al-'alqami river water treatment. Journal of Natural Sciences Research 5: 125–13551.

48. Priebe M., Fromm K. M. (2014). Nanorattles or yolk-shell nanoparticles-what are they, how are they made, and what are they good for?. Chemistry - A European Journal 21: 3854–3874.

49. Hayes R., Ahmed A., Edge T., Zhang H. (2014). Core-shell particles: preparation, fundamentals and applications in high performance liquid chromatography. Journal of Chromatography A 1357: 36–52.

50. Purbia R., Paria S. (2015). Yolk/shell nanoparticles: classifications, synthesis, properties, and applications. Nanoscale 7: 19789-197873.

51. Zhang L., Yang X., Han E., Zhao L., Lian J. (2016). Reduced graphene oxide wrapped Fe3O4–Co3O4 yolk–shell nanostructures for advanced catalytic oxidation based on sulfate radicals. Applied Surface Science.

52. Ito A., Shinkai M., Honda H., Kobayashi T. (2005). Medical application of functionalized magnetic nanoparticles. Journal of bioscience and bioengineering. 100:1–11.

53. Châtel P. F. de, Nándori I., Hakl J., Mészáros S., Vad K.. (2009). Magnetic particle hyperthermia: Néel relaxation in magnetic nanoparticles under circularly polarized field. Journal of Physics 21: 8.

54. Chowdhury S., YusofF., Salim W. W. A. W., Sulaiman N., Faruck, M. O. (2016). An overview of drug delivery vehicles for cancer treatment: Nanocarriers and nanoparticles including photovoltaic nanoparticles. Journal of Photochemistry and Photobiology B: Biology 164: 151–159.

55. Singh R., Lillard J. W. (2009). Nanoparticle-based targeted drug delivery. Experimental and Molecular Pathology 86: 215–223.

56. Du J., Du X., Mao C., Wang, J. (2011) Tailor-made dual pH-sensitive polymer-doxorubicin nanoparticles for efficient anticancer drug delivery. Journal of the American Chemical Society 133: 17560–175633.

57. Shen H., Zhang L., Liu M., Zhang Z. (2012). Biomedical applications of graphene. Theranostics 2: 283–294.

58. Righetto, L. Doxorrubicina - Bula Doxorrubicina. (2013). Available at: http://www.medicinanet.com.br/bula/2080/doxorrubicina.htm. (Accessed: 23rd January 2017).

59. Cancer. World Health Organization (WHO) (2017). Available at: http://www.who.int/mediacentre/factsheets/fs297/en/. (Accessed: 26th February 2017).

60. Martins A., Barros L., Carvalho A. M., Santos-Buelga C., Fernandes I. P., Barreiro F., Ferreira I. C. F. R. (2014). Phenolic extracts of Rubus ulmifolius Schott flowers: characterization, microencapsulation and incorporation into yogurts as nutraceutical sources. Food & Function 5: 1091–1100.

61. Ferreira I. C. F. R., Baptista P., Vilas-boas M., Barros L. (2007). Free-radical scavenging capacity and reducing power of wild edible mushrooms from northeast Portugal : Individual cap and stipe activity. Food Chemistry 100: 1511–1516.

62. Ribeiro R. S., Rodrigues R.O., Silva A. M. T., Tavares P. B., Carvalho A.M.C., Figueiredo J.L., Faria J.L., Gomes H.T. (2017). Hybrid magnetic graphitic nanocomposites towards catalytic wet peroxide oxidation of the liquid effluent from a mechanical biological treatment plant for municipal solid waste. Applied Catalysis B: Environmental 219: 645–657.

63. Lim D. J., Sim M., Oh, Lim K., Park H. (2013). Carbon-based drug delivery carriers for cancer therapy. Archives of Pharmacal Research

64. Cha C., Shin S. R., Annabi N., Dokmeci M. R., Khademhosseini A. (2013). Carbon-based nanomaterials: multi-functional materials for biomedical engineering. ACS Nano 7: 2891–2897.

65. Bagavathi M., Ramar A., Saraswathi, R. (2016). Fe3O4–carbon black nanocomposite as a highly efficient counter electrode material for dye-sensitized solar cell. Ceramics International 42:13190–13198.

66. Wang H., Chen Q.-W., Chen J., Yu B.-X., Hu X.-Y. (2011). Carboxyl and negative charge-functionalized superparamagnetic nanochains with amorphous carbon shell and magnetic core: synthesis and their application in removal of heavy metal ions. Nanoscale 3: 4600.

Annex A

Figures I to VIII show the equipment used during the experiments.

Figure I - Magnetic stirring plate IKA® C-MAG HS 7 with temperature control IKA® ETS-D5.

Figure II - Peristaltic pump ISM 845, ISMATEC.

Figure III - Centrifugal MPW-260R, MPW Med. Instruments.

Figure IV - Drying oven FD 115, Binder.

Figure V - Ultrasons-H, P-Selecta.

Figure VI - Vertical tubular furnace ROS 50/250/12, Thermoconcept.

Figure VII - Orbital shaker IKA® KS 130 basic.

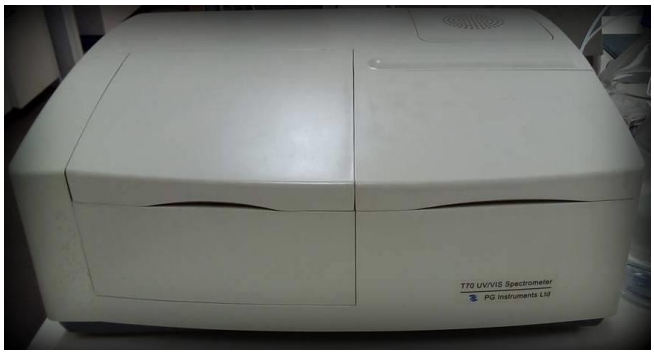

Figure VIII - T70 UV-VIS spectrophotometer, PG Instruments Ltd.